

9-6-2022

## Artificial gravity partially protects space-induced neurological deficits in *Drosophila melanogaster*

Siddhita D. Mhatre  
*NASA Ames Research Center*

Janani Iyer  
*NASA Ames Research Center*

Juli Petereit  
*University of Nevada, Reno*

Roberta M. Dolling-Boreham  
*McMaster University*

Anastasia Tyryshkina  
*Pennsylvania State University*

*See next page for additional authors*

Follow this and additional works at: [https://scholarworks.sjsu.edu/faculty\\_rsca](https://scholarworks.sjsu.edu/faculty_rsca)

---

### Recommended Citation

Siddhita D. Mhatre, Janani Iyer, Juli Petereit, Roberta M. Dolling-Boreham, Anastasia Tyryshkina, Amber M. Paul, Rachel Gilbert, Matthew Jensen, Rebekah J. Woolsey, Sulekha Anand, Marianne B. Sowa, David R. Quilici, Sylvain V. Costes, Santhosh Girirajan, and Sharmila Bhattacharya. "Artificial gravity partially protects space-induced neurological deficits in *Drosophila melanogaster*" *Cell Reports* (2022).  
<https://doi.org/10.1016/j.celrep.2022.111279>

This Article is brought to you for free and open access by SJSU ScholarWorks. It has been accepted for inclusion in Faculty Research, Scholarly, and Creative Activity by an authorized administrator of SJSU ScholarWorks. For more information, please contact [scholarworks@sjsu.edu](mailto:scholarworks@sjsu.edu).

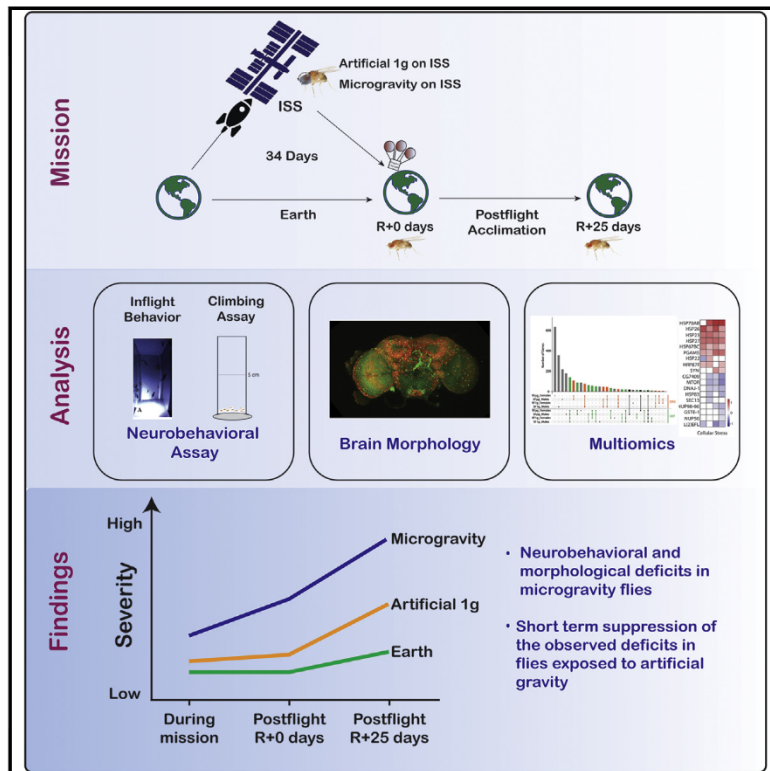
---

**Authors**

Siddhita D. Mhatre, Janani Iyer, Juli Petereit, Roberta M. Dolling-Boreham, Anastasia Tyryshkina, Amber M. Paul, Rachel Gilbert, Matthew Jensen, Rebekah J. Woolsey, Sulekha Anand, Marianne B. Sowa, David R. Quilici, Sylvain V. Costes, Santhosh Girirajan, and Sharmila Bhattacharya

## Artificial gravity partially protects space-induced neurological deficits in *Drosophila melanogaster*

### Graphical abstract



### Authors

Siddhita D. Mhatre, Janani Iyer, Juli Petereit, ..., Sylvain V. Costes, Santhosh Girirajan, Sharmila Bhattacharya

### Correspondence

sharmila.bhattacharya@nasa.gov

### In brief

Mhatre et al.'s ISS-based multi-modal study provides insights into CNS responses to spaceflight and evaluates artificial gravity (AG) as a potential countermeasure. AG provides partial protection to the neurological deficits observed in flies reared in spaceflight microgravity ( $SF_{\mu}g$ ); the deficits progressively worsen with postflight acclimation to Earth conditions.

### Highlights

- Spaceflight microgravity ( $SF_{\mu}g$ ) flies show CNS deficits and gene-expression changes
- Cellular stress and metabolic reprogramming responses observed in spaceflight flies
- Acclimation of space flies to Earth show brain deficits that are more severe in  $SF_{\mu}g$
- Artificial gravity partially protects the CNS from the adverse effects of spaceflight



## Article

# Artificial gravity partially protects space-induced neurological deficits in *Drosophila melanogaster*

Siddhita D. Mhatre,<sup>1,2,3,14</sup> Janani Iyer,<sup>1,2,4,14</sup> Juli Petereit,<sup>5</sup> Roberta M. Dolling-Boreham,<sup>6,7</sup> Anastasia Tyryshkina,<sup>8</sup> Amber M. Paul,<sup>1,4,7,9,12</sup> Rachel Gilbert,<sup>1,9</sup> Matthew Jensen,<sup>8</sup> Rebekah J. Woolsey,<sup>10</sup> Sulekha Anand,<sup>11</sup> Marianne B. Sowa,<sup>1</sup> David R. Quilici,<sup>10</sup> Sylvain V. Costes,<sup>1</sup> Santhosh Girirajan,<sup>8</sup> and Sharmila Bhattacharya<sup>1,13,15,\*</sup>

<sup>1</sup>Space Biosciences Division, NASA Ames Research Center, Moffett Field, CA 94035, USA

<sup>2</sup>KBR, NASA Ames Research Center, Moffett Field, CA 94035, USA

<sup>3</sup>COSMIAC Research Center, University of New Mexico, Albuquerque, NM 87131, USA

<sup>4</sup>Universities Space Research Association, Mountain View, CA 94043, USA

<sup>5</sup>Nevada Bioinformatics Center, University of Nevada, Reno, NV 89557, USA

<sup>6</sup>Department of Electrical and Biomedical Engineering, McMaster University, Hamilton, ON L8S 4L8, Canada

<sup>7</sup>Blue Marble Space Institute of Science, Seattle, WA 94035, USA

<sup>8</sup>Department of Biochemistry & Molecular Biology, Pennsylvania State University, University Park, PA 16802, USA

<sup>9</sup>NASA Postdoctoral Program, Universities Space Research Association, NASA Ames Research Center, Moffett Field, CA 94035, USA

<sup>10</sup>Nevada Proteomics Center, University of Nevada, Reno, NV 89557, USA

<sup>11</sup>Department of Biological Sciences, San Jose State University, San Jose, CA 95192, USA

<sup>12</sup>Embry-Riddle Aeronautical University, Department of Human Factors and Behavioral Neurobiology, Daytona Beach, FL 32114, USA

<sup>13</sup>Biological and Physical Sciences Division, NASA Headquarters, Washington DC 20024, USA

<sup>14</sup>These authors contributed equally

<sup>15</sup>Lead contact

\*Correspondence: [sharmila.bhattacharya@nasa.gov](mailto:sharmila.bhattacharya@nasa.gov)

<https://doi.org/10.1016/j.celrep.2022.111279>

## SUMMARY

Spaceflight poses risks to the central nervous system (CNS), and understanding neurological responses is important for future missions. We report CNS changes in *Drosophila* aboard the International Space Station in response to spaceflight microgravity (SF $\mu$ g) and artificially simulated Earth gravity (SF1g) via inflight centrifugation as a countermeasure. While inflight behavioral analyses of SF $\mu$ g exhibit increased activity, postflight analysis displays significant climbing defects, highlighting the sensitivity of behavior to altered gravity. Multi-omics analysis shows alterations in metabolic, oxidative stress and synaptic transmission pathways in both SF $\mu$ g and SF1g; however, neurological changes immediately postflight, including neuronal loss, glial cell count alterations, oxidative damage, and apoptosis, are seen only in SF $\mu$ g. Additionally, progressive neuronal loss and a glial phenotype in SF1g and SF $\mu$ g brains, with pronounced phenotypes in SF $\mu$ g, are seen upon acclimation to Earth conditions. Overall, our results indicate that artificial gravity partially protects the CNS from the adverse effects of spaceflight.

## INTRODUCTION

Exploration missions to the Moon and Mars would expose astronauts to environmental challenges, including gravitational changes, ionizing radiation, altered circadian rhythm, elevated CO<sub>2</sub>, and isolation. Human acclimation to these environments presents complex health effects, with acute and prolonged consequences in multiple tissues that may result in increased risk to crew health and performance during the mission (Afshinnkoo et al., 2020; Crucian et al., 2015; Garrett-Bakelman et al., 2019; Grimm et al., 2016; Indo et al., 2016; Kononikhin et al., 2017; Wilson et al., 2018). With a high concentration of oxidizable, unsaturated lipids, low levels of antioxidant defenses, and high energy demand, the central nervous system (CNS) is

particularly vulnerable to space stressors, with studies reporting behavioral deficits in spatial orientation, coordination, and locomotion, as well as cognition (Cekanaviciute et al., 2018; Clément et al., 2020; Salim, 2017; Friedman, 2011).

Spanning over 60 years of research, the short-term impacts of spaceflight on the CNS have been investigated, but there is still insufficient data regarding its long-term health risks (Clément et al., 2020). Also, there are limitations to evaluating the impact of CNS damage in humans. Therefore, there is a need to leverage research approaches using animal models that would aid in cellular, molecular, and mechanistic understanding of CNS responses to spaceflight. Recent literature has established the fruit fly as a valuable model for understanding the effects of microgravity ( $\mu$ g), hypergravity, and radiation in the spaceflight



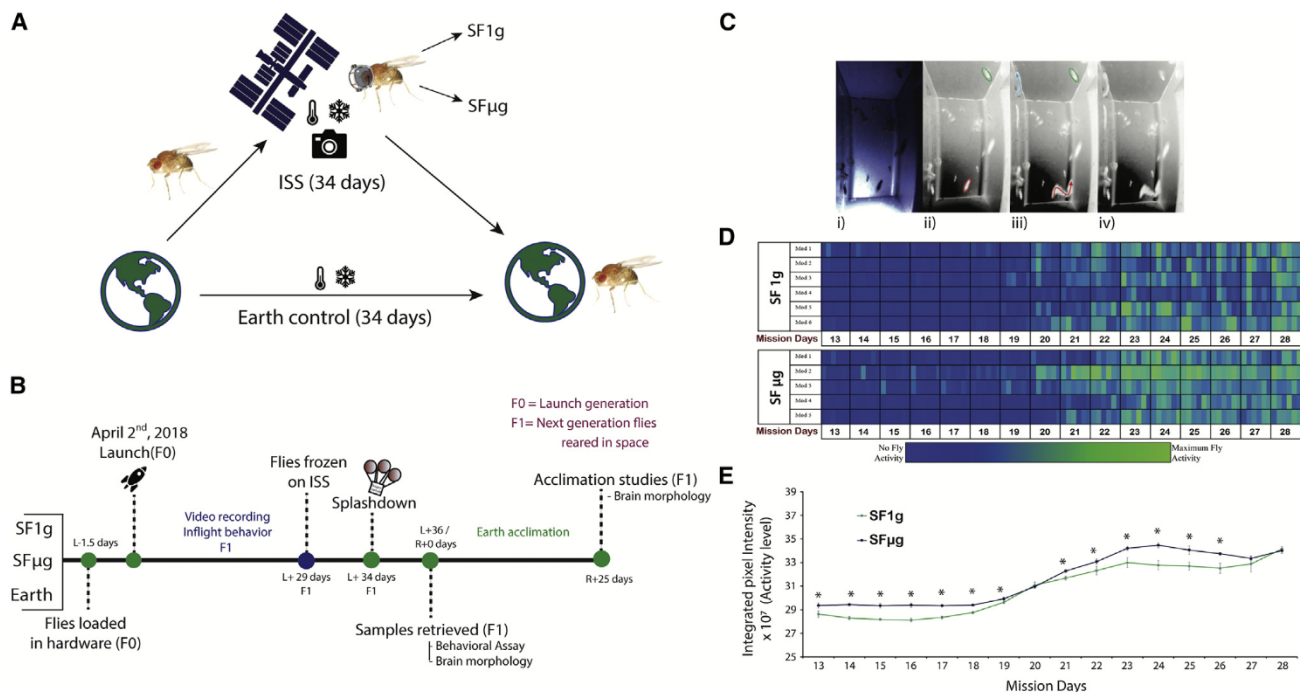


**Figure 1. Inflight behavioral analysis shows hyperactivity in microgravity**

(A) Schematic of MVP-Fly01 mission outline depicting the 34-day mission on ISS. Camera represents inflight videos that were recorded to monitor fly health and behavior. Onboard operations included freezing the food cylinders containing flies and larvae in RNAlater for omics analysis. Live flies were returned to Earth. Following the telemetry and timeline of the mission, matched Earth controls were performed (Earth).

(B) Experimental timeline highlighting the onboard operations and postflight R+0 and R+25 assays.

(C) Computation of fly activity by MIP. (i) The first frame from one video recorded during the mission. (ii) The negative of the blue channel in grayscale of the first frame with two flies circled in green and red. (iii) The MIP image captures the movement (blue and red arrows) and no movement (green) of the flies. (iv) Final MIP projection used in the algorithm. The white tracks represent flies that moved at any point during the recording.

(D) Fly activity mapped overtime for 16 days (mission days 13–28). Each row represents one adult fly chamber in an individual MVP module, and across from left to right is a temporal progression with every six rectangles (each rectangle = 28-s video recording) spanning a single 12-h light period. The color bar represents the activity level from a minimum background intensity (dark blue) to the highest activity level intensity (bright green). Top six rows correspond to SF1g flies and the bottom five to SF $\mu$ g flies.

(E) Line graphs show increased activity levels across mission days 13–28 averaged over each day across modules for each population set (n = 5–73). \*p < 0.05. Error bars represent SEM.

environment (Hateley et al., 2016; Hosamani et al., 2016; Ikenaga et al., 1997; Marcu et al., 2011; Ogneva et al., 2016). With their small size, short generation time (~10 days), short lifespan (~60–80 days), large number of offspring, and low cost of rearing, flies mitigate many of the practical concerns stemming from performing long-term, multi-generational studies in space.

Here, we present the results of an International Space Station (ISS)-based study, Multi-use Variable-gravity Platform (MVP)-Fly-01, to understand the effects of spaceflight on the fly nervous system and the value of artificial gravity (AG) as a countermeasure. AG is an attractive countermeasure since it can potentially ameliorate the effect of  $\mu$ g on multiple physiological systems by simulating Earth-like gravity (Clément, 2017; Clément and Traon, 2004; Horie et al., 2019; Shiba et al., 2017; Young, 1999). We performed behavioral analyses, brain immunohistochemistry, proteomics, and transcriptomics on flies subjected to spaceflight microgravity (SF $\mu$ g), inflight artificially simulated Earth gravity (SF1g), and environmentally matched ground control (Earth). Our results showed inflight and postflight behavioral changes and morphological alterations in the brain immediately postflight

in response to  $\mu$ g. Further, acclimation to Earth following spaceflight revealed brain morphological changes in both SF1g and SF $\mu$ g flies, with pronounced phenotypes in SF $\mu$ g. These results, in combination with metabolic pathways altered in transcriptional and proteomic studies on fly heads frozen on the ISS, provide comprehensive information on the effects of inflight AG exposure on CNS and postflight acclimation to Earth conditions.

## RESULTS

### The MVP-Fly-01 mission

The ISS is a useful environment for studying the effects of spaceflight by combining a  $\mu$ g environment with ionizing radiation and CO<sub>2</sub> levels that are elevated compared with Earth's surface (McDonald et al., 2020). The MVP-Fly-01 validation mission (34 days) has enabled comprehensive investigations of the fly CNS (Figure 1A). The two inflight centrifuges in the MVP hardware allowed us to maintain one centrifuge at  $\mu$ g (SF $\mu$ g) with the flies developing entirely in  $\mu$ g, while the other centrifuge simulated Earth's gravitational force (SF1g) on ISS and acted as a

high-fidelity, on-orbit control for gravity. In other words, the spaceflown flies experienced identical environmental perturbations during takeoff and landing and were maintained in identical hardware and similar gas composition, sound pressure levels, temperature, and radiation environments in space but were reared either under a 1g force in space or in  $\mu\text{g}$ . Upon completing the mission, a post-flight ground control experiment was performed on Earth (Earth) using the same flight hardware and precisely simulating spaceflight conditions. The flies retrieved upon completion of the mission were used for behavioral, morphological, and acclimation analyses to study the effects of spaceflight on the CNS (Figure 1B).

### SF $\mu\text{g}$ flies exhibit increased activity on ISS

We developed an automated quantification algorithm that computes the maximum intensity projections (MIPs) of video recordings of fly behavior (represented in Videos S1 and S2) during spaceflight and sums pixel intensities to produce numerical values representative of fly activity levels (higher numerical values correlate with high fly activity), accounting for both the emergence of flies and their movement during the 12-h light period (Figure 1C). Since the fly population sizes in adult fly chamber 1 were not statistically different between SF1g and SF $\mu\text{g}$  (Figure S2), any difference in MIP intensity between these two groups reflected differences in fly activity. We generated a color map showing the relative numerical activity in adult fly chamber 1 as a function of mission timeline (days 13–28) for each module grouped as either SF1g or SF $\mu\text{g}$  (Figure 1D). Upon quantification, we found that the overall activity level of the SF1g flies is significantly below SF $\mu\text{g}$  flies (Figure 1E). On mission days 20 and 28, there is no distinguishable difference in the activity for the two gravity levels. This is possibly due to the initial emergence of flies into the adult fly chamber around day 20 that causes a similar increase in activity in both SF1g and SF $\mu\text{g}$  environments. On day 28, the high density of flies in both conditions may result in close proximity of the flies, thereby increasing their activity levels. The results show that within the closely matched fly populations maintained in spaceflight, flies exposed to  $\mu\text{g}$  conditions show significantly greater levels of activity than their 1g counterparts.

### Flies exposed to $\mu\text{g}$ conditions show behavioral and neuronal deficits, glial alterations, oxidative damage, and apoptosis

Upon landing, a subset of F1 flies were first used for behavioral assays to measure climbing ability. Climbing ability is the fly's innate negative geotactic response and is routinely used to assess nervous system dysfunction in fly models (Chakraborty et al., 2011; Iijima et al., 2004). This behavior relies on the integrity of the connection between the brain and muscles. Specifically, it involves the mushroom body, which is the part of the brain that regulates the transition from rest to responsiveness in relation to environmental stressors (Martin et al., 1998). To capture the sexually dimorphic responses, we assessed males and females separately in our analysis. We observed that males born in  $\mu\text{g}$  were more affected with significant deficits in climbing ability compared with Earth males (Figure 2A). A decreasing trend was also observed in SF $\mu\text{g}$  females and SF1g (males and females) compared with their respective Earth control. Additionally, we noted a significant decrease in climbing ability in SF $\mu\text{g}$

males compared with SF $\mu\text{g}$  females. This result is consistent with the previously observed reduction in postflight climbing response in males exposed to  $\mu\text{g}$  (Benguría et al., 1996).

We then dissected the adult fly brains and stained them with neuronal (anti-ELAV) (Figure 2B), apoptotic (anti-CC3), and oxidative stress-associated DNA damage (anti-8-oxo-dG) (Figure 2E) markers. Upon quantification, we observed a slight yet significant reduction in the total brain area of SF $\mu\text{g}$  female flies compared with both Earth and SF1g females; males showed no change in brain sizes (Figure S3A). Morphological quantification with anti-ELAV staining showed a significant decrease in neuronal cortex area (Figures 2B, 2C, and S3B) in SF $\mu\text{g}$  flies compared with Earth and SF1g control flies in both sexes. Similarly, the neuropil area is significantly reduced in SF $\mu\text{g}$  compared with Earth flies (Figure 2D). A similar phenotype was noted in the Alzheimer's disease fly model accompanied by behavioral deficits (Mhatre et al., 2014). No significant differences in neuronal cortex and neuropil areas were observed in SF1g compared with Earth flies (Figures 2C and 2D). A marked increase in CC3-positive apoptotic puncta (Figures 2E and 2H) and 8-oxo-dG-positive cells (Figures 2E and 2I) was observed in flies subjected to SF $\mu\text{g}$  compared with Earth and SF1g controls. Apoptotic cells were detected throughout the brain, and many of them colocalized with the ELAV marker (Figure S3Cv). Additionally, all the 8-oxo-dG-positive cells colocalize with neuronal ELAV marker, suggesting oxidative damage in neuronal cells (Figure S3Civ, marked with green arrowhead). The observed oxidative stress response has been documented in previous spaceflight and ground-based altered gravity studies in mice and flies (Hateley et al., 2016; Hosamani et al., 2016; Mao et al., 2016, 2018b, 2020; da Silveira et al., 2020).

Another subset of brains was stained with glial (anti-repo) and dopaminergic neuron (anti-TH) (Figure 2E) markers. Gross analysis of the total number of dopaminergic (DA) neurons revealed a reduction in DA neuron count in SF $\mu\text{g}$  compared with SF1g and Earth fly brains in both sexes (Figures 2E and 2F). Like the climbing behavior, we observed significantly lowered DA neurons in SF $\mu\text{g}$  males compared with SF $\mu\text{g}$  females, suggesting sensitivity of male flies to  $\mu\text{g}$ . DA neurons are involved in locomotion, and the lack of these neurons has been identified in the development of Parkinson's disease in humans (Ryczko and Dubuc, 2017). We also observed a significant increase in DA neurons in SF1g males compared with the Earth males; this may be part of a phenotype resulting from exposure to a 1g centrifugal force on flies that are also perturbed by a combination of spaceflight stressors—ionizing radiation and elevated CO<sub>2</sub> levels. In the case of glia, SF $\mu\text{g}$  females and SF1g (both males and females) displayed an increasing trend in glial cell number compared with Earth controls. However, the SF $\mu\text{g}$  males showed a decreasing trend in the glial population compared with Earth males (Figure 2E and 2G) and a significant reduction in the glial population compared with SF1g males. Further experiments are necessary to study the sex specificity of the spaceflight effects and the underlying mechanisms contributing to these differences in glial cell populations.

The SF1g and Earth flies were exposed to similar temperature, humidity, CO<sub>2</sub>, and sound pressure levels; however, ionizing radiation was an additional spaceflight stressor experienced by the SF1g flies compared with the Earth flies. Thus, the similarity in morphological phenotype between SF1g and Earth control flies

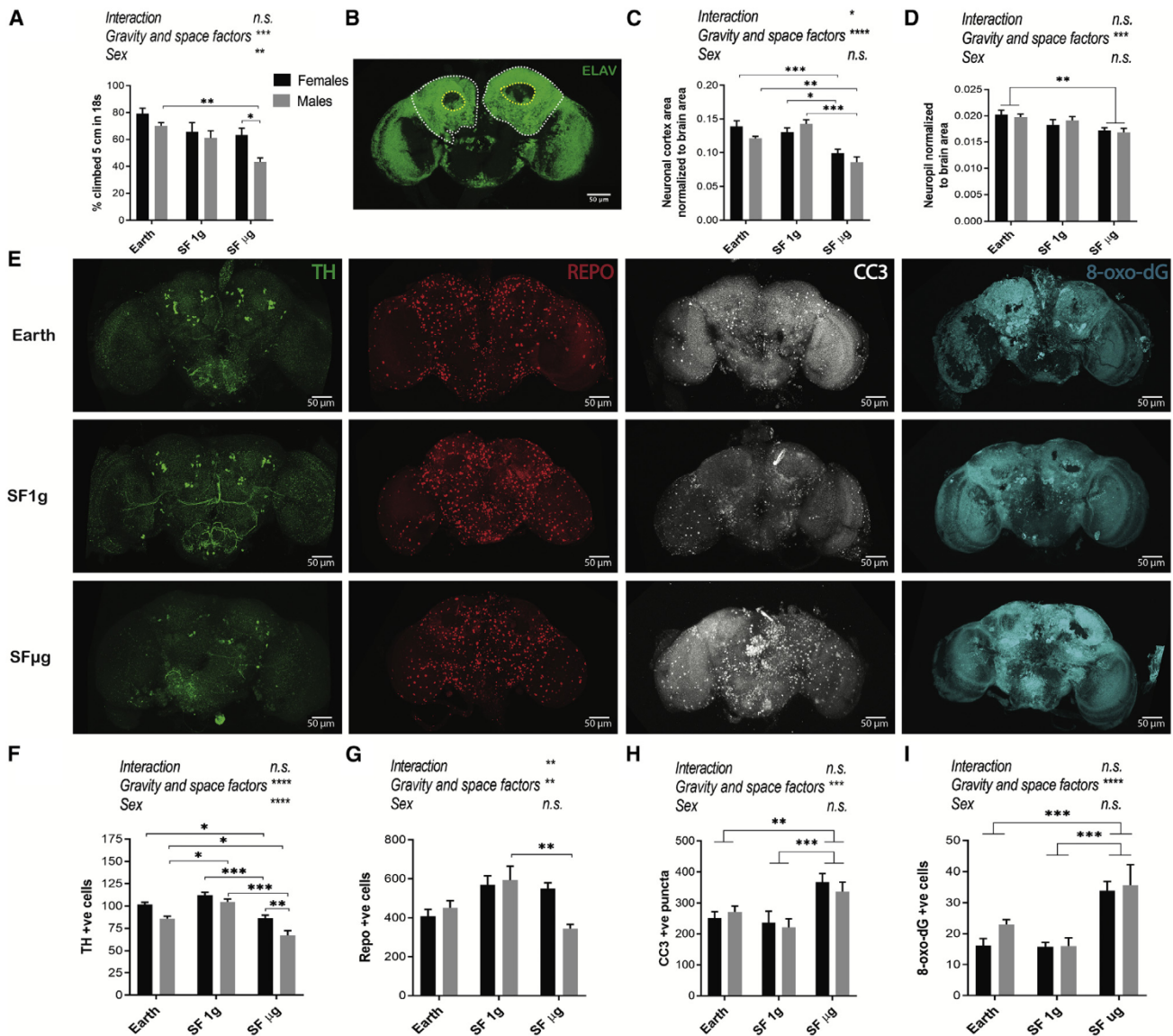


**Figure 2. CNS-associated deficits in microgravity flies**

(A) Decreased climbing ability of space-flight flies (n = 90–120).

(B) Representative image of fly brain stained with neuronal marker anti-ELAV; neuronal cortex marked by the dashed outer white line and neuropil marked by the dashed inner yellow line.

(C and D) Quantification shows decrease in neuronal cortex area (C) and neuropil area (D) in SF1μg compared with both Earth and SF1g controls (n = 10–14).

(E) Representative images of fly brains labeled with anti-TH (green), anti-repo (red), anti-CC3 (white), and anti-8-oxo-dG (cyan).

(F–I) Quantification showed significant loss in DA neurons (F) (n = 6–9) and alterations in glial numbers (G) (n = 5–9), apoptosis (H) (n = 5–7), and oxidative DNA damage (I) (n = 5–7) in SF1μg condition. Two-way ANOVA results are displayed above the histogram. Significance calculated by post-hoc test is represented as \*p < 0.05; \*\*p < 0.01; \*\*\*p < 0.001. Scale bar represents 50 microns. Error bars represents SEM.

in many of the readouts analyzed here, including behavior, neuronal cortex and neuropil areas, apoptosis, and oxidative damage (Figure 2), suggests that radiation alone may not be a significant contributing factor for the immediate postflight CNS effects of spaceflight. However, ionizing radiation may contribute to some of the long-term effects of spaceflight on the CNS and are discussed further in a later section. The entire experiment occurred over a short duration (34 days), and the radiation envi-

ronment in low-Earth orbit (LEO) is known to be more benign than the environment in deep space, beyond the Van Allen belts (Nelson, 2016). Therefore, the gross physiological changes induced in LEO flights like on the ISS, as observed in SF1μg flies, at least for the CNS immediately postreturn, may primarily be associated with changes in gravity. Thus, these results indicate that gravity can play a key role in the LEO environment, causing neuronal and neurobehavioral deficits during spaceflight.

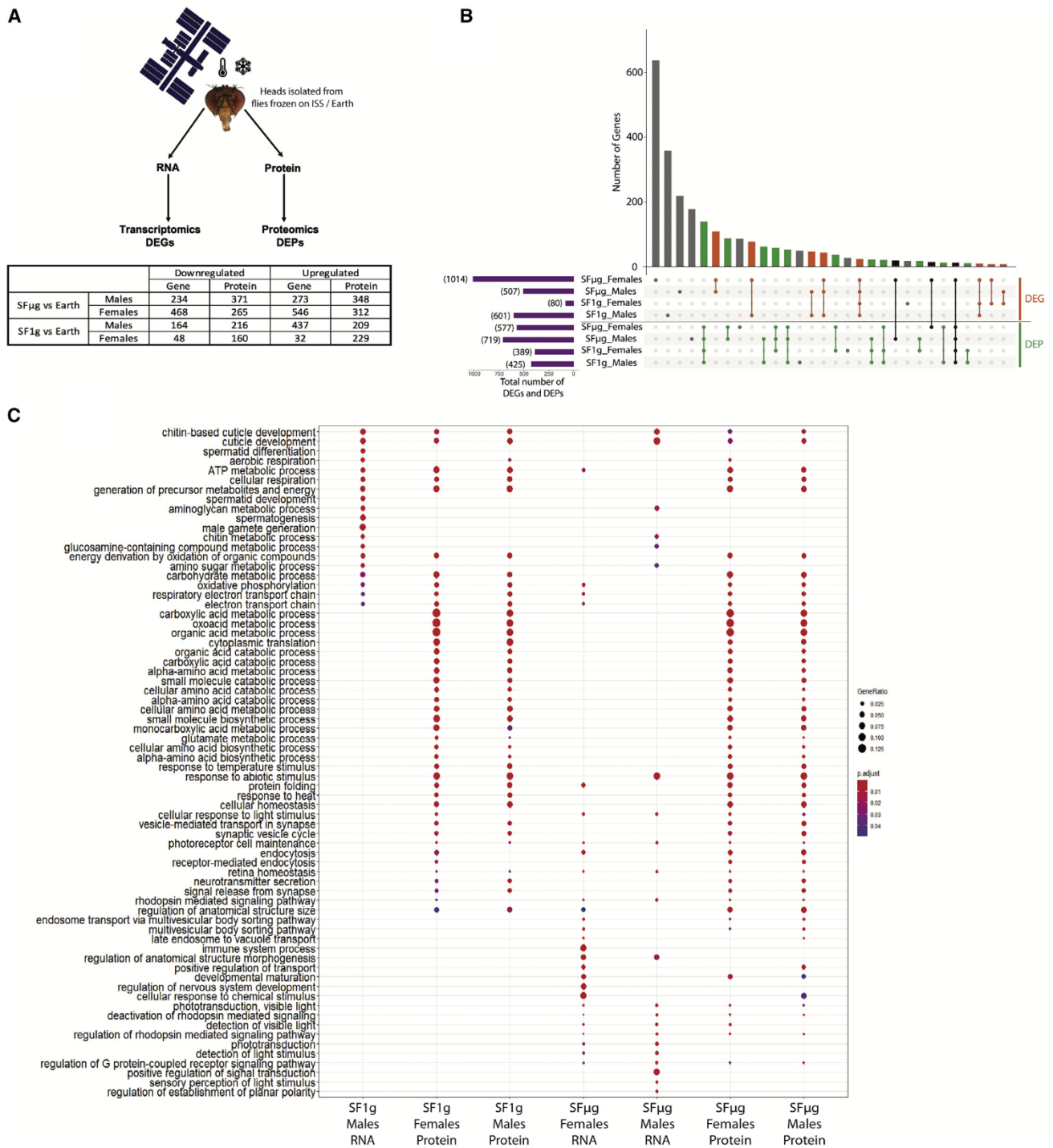


**Figure 3. Global overview of multi-omics analysis on flies frozen in space**

(A) Schematic showing transcriptomics and proteomics sample processing. Table provides a global view of the total number of differentially up- and down-regulated genes (DEGs) and proteins (DEPs) in SF1g and SF $\mu$ g compared with Earth control.

(B) Upset plot displays top 30 intersections across omics platforms and between conditions (SF1g males, SF1g females, SF $\mu$ g males, SF $\mu$ g females). The purple horizontal bars indicate the total number of DEGs and DEPs identified in each condition. The dotted region shows all conditions, and connecting lines with black nodes show overlap across omics platforms (DEGs and DEPs), whereas orange nodes show overlap across different conditions in DEGs and green nodes show

(legend continued on next page)



### Global omics analysis highlights spaceflight-induced altered genes and proteins in the brain

Transcriptomics and proteomics analyses were performed on the heads of flies that were developed entirely on ISS under SF $\mu$ g or SF1g conditions and Earth controls (Figure 3A). RNA sequencing (RNA-seq) on heads from SF $\mu$ g flies compared with Earth controls showed differential expression of 1,014 genes in females and 507 genes in males, while proteomics analysis revealed differential expression of 577 proteins in females and 719 proteins in males. RNA-seq in SF1g flies compared with Earth-reared flies showed differential expression of 80 genes in females and 601 genes in males, and proteomics analysis revealed differential expression of 389 proteins in females and 425 proteins in males (Figure 3A). Overall, these results suggest alterations in transcripts and protein levels when flies are reared in space conditions compared with in Earth condition. A full list of differentially expressed genes (DEGs) and differentially expressed proteins (DEPs) is provided in Tables S1 and S2. Further, to understand the overlap across the transcriptomics and proteomics as well as across the different experimental conditions, we generated an UpSet diagram displaying top 30 intersections (Figure 3B). The overlap between the DEGs (orange dots and bars) and DEPs (green dots and bars) for the experimental conditions is shown and across DEGs and DEPs are marked in black. Also shown are the genes and proteins unique to each condition (gray dots and bars). The intersection within DEPs across experimental conditions yields more hits compared with DEGs. This is evidenced by 167 significantly altered proteins (adjusted p value [adj. p] < 0.05) compared with 25 significantly altered genes (adj. p < 0.05) in SF1g and SF $\mu$ g conditions compared with Earth controls (Figures 3B, S4A, and S4B). The observed overlapping DEPs and DEGs are potential spaceflight signatures irrespective of gravity that can be further investigated. Additionally, though we observe minimal overlap across both transcriptomic and proteomic platform, the common processes possibly share a transcriptional mechanism of dysregulation, hence making these processes central towards the phenotype manifested in spaceflight flies. For example, as shown in the case of SF $\mu$ g females compared with Earth females, the Gene Ontology (GO) analysis of overlapping DEPs and DEGs (65) revealed enrichment of key biological processes (BPs), cellular components (CCs), and molecular functions (MFs) that closely regulate mitochondrial functions, metabolic processes, immune response, and synaptic signaling, among others (Figure S4C).

### Focused analysis reveals differential alteration in metabolic pathways and oxidative phosphorylation in space-reared flies

The spaceflight conditions (SF1g and SF $\mu$ g) compared with Earth were analyzed across the omics platforms. Figure 3C highlights the top 20 significantly enriched GO BPs, including cuticle development, oxidative phosphorylation, electron transport chain,

metabolic processes, response to heat, protein folding, neurotransmitter secretion, synaptic vesicle signaling, and retinal homeostasis, among others. The enrichment is more evident in proteins compared with RNA. The complete list from GO enrichment analysis (BPs, CCs, MFs) is provided in Tables S1 and S2. Further, we note a sexually dimorphic response in the transcriptomic dataset, which is not observed in proteomics analysis (Figure S5).

KEGG pathway enrichment analysis on the proteomics dataset across conditions revealed sexual dimorphism at the pathway enrichment level (more KEGG pathway enrichment in females than males), which was more evident in SF1g than SF $\mu$ g conditions. Proteomic data of SF $\mu$ g flies (males and females) show enrichment of pathways such as endocytosis and cellular metabolic responsive pathways—tyrosine metabolism, sucrose metabolism, pyruvate metabolism, oxidative phosphorylation, carbon metabolism, glutamate metabolism, glycolysis, fatty acid metabolism, and amino acid metabolism (Figure 4A). These metabolic pathways play critical roles in cellular as well as mitochondrial homeostasis. The metabolic reprogramming under spaceflight conditions suggests metabolic and cellular stress, similar to that observed in cancer and aging (Brooks Robey et al., 2015; Wallace, 2005). Similar regulation of metabolic pathways is observed in other spaceflight-based mammalian studies, including humans (Garrett-Bakelman et al., 2019; de Luca et al., 2009; da Silveira et al., 2020; Stein, 2002). Analysis of cellular respiration revealed perturbations in the BPs and CCs encompassing every step of the pathway, i.e., glucose metabolism, pyruvate metabolism, citric acid cycle (TCA), and electron transport chain as well as at mitochondrial organelle level (Figures 4B and 4C). This is observed in both spaceflight conditions but is more pronounced in SF $\mu$ g than SF1g (both sexes), suggesting differential regulation under the spaceflight stress  $\pm$  gravity vector.

At the mitochondrial level, an increase in PGAM5 and mitochondrial fission/fusion proteins such as dynamin-related protein 1 (DRP1) and OPA1 were observed, suggesting increased mitochondrial dynamics (Figure 4D). We observed the upregulation of many enzymes involved in glycolysis, such as hexokinase C (HEXC) and fructose 1,6-bisphosphatase (FBP) (Figure 4E), suggesting increased glycolytic flux (Tanner et al., 2018). Meanwhile, we observed an increase in lactate dehydrogenase (LDH), suggesting funneling of glycolysis products toward lactate production under spaceflight conditions. Another key enzyme, AcCoAS, is downregulated, thereby reducing the production of acetyl-coenzyme A (CoA), a key enzyme required for the TCA cycle. Further, modulation of proteins involved in oxidative phosphorylation/electron transport chain (ETC) is noted (Figure 4F). While ETC proteins are differentially regulated under both SF1g and SF $\mu$ g conditions, the number of proteins dysregulated under SF $\mu$ g is more than the SF1g condition. In fact, differential regulation of at least one protein associated with each of the five ETC complexes is observed under SF $\mu$ g conditions (Figure 4G), which may contribute to

overlap across different conditions in DEPs. Gray nodes represent the DEGs and DEPs unique to a condition. The vertical bars indicate the number of unique or overlapping genes/proteins.

(C) Dot plot representing top 20 significantly (adj. p < 0.05) enriched Gene Ontology (GO) terms in biological processes in SF1g and SF $\mu$ g compared with Earth control. SF1g female RNA compared with Earth control did not have any enriched GO biological processes, hence they are not represented in the dot plot. The color of the dot represents the adj. p value, and the size represents gene ratio.

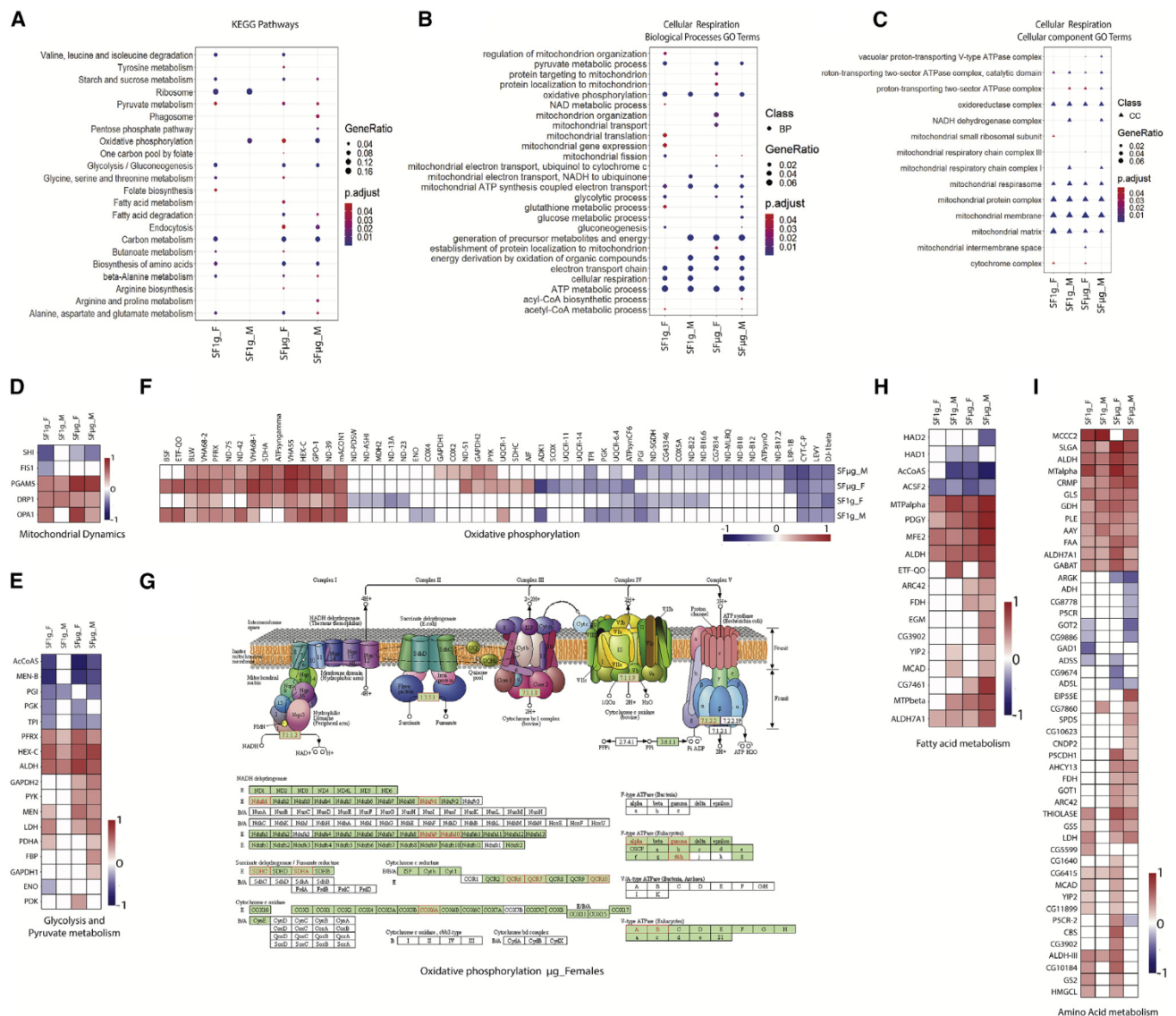


**Figure 4. Metabolic pathways and cellular respiration affected by spaceflight**

(A) Dot plot representing the KEGG pathways ( $p < 0.05$ ) enriched in DEPs across different conditions. The size of the dot is based on the gene count enriched in the pathways, and the color of the dot represents pathway significance.

(B and C) GO enrichment analysis. Dot plot showing GO terms (adj.  $p < 0.05$ ) associated with cellular respiration in biological processes (B) and cellular components (C) for SF1g and SF $\mu\text{g}$  (DEPs) compared with Earth control. The color of the dot represents the adj.  $p$  value, and the size represents gene ratio.

(D–F) Heatmap representation of differential expression ( $\log_2$ [fold change]) of significantly altered (adj.  $p < 0.05$ ) mitochondrial fusion/fission proteins (D), glycolysis and pyruvate metabolism proteins (E), and proteins associated with oxidative phosphorylation (F) in SF1g and SF $\mu\text{g}$  versus Earth.

(G) Differentially expressed proteins (in red) in SF $\mu\text{g}$  females (versus Earth females) are mapped onto the oxidative phosphorylation KEGG pathway using KEGG mapper.

(H and I) Heatmap displays  $\log_2$ [fold change] of proteins that are significantly expressed (adj.  $p < 0.05$ ) in fatty acid metabolism (H) and amino acid metabolism (I), with red representing upregulated and blue for downregulated.

reactive oxygen species (ROS) production. Moreover, KEGG pathway enrichment shows differential regulation of fatty acid metabolism as well as amino acid metabolism. We observed an upregulation of enzymes involved in fatty acid (Figure 4H) and amino acid metabolism (Figure 4I), suggesting high energy demand, thereby emphasizing cellular stress response under spaceflight conditions (SF $\mu\text{g}$  > SF1g).

### Spaceflight alters the expression of stress-inducible proteins affecting CNS

During spaceflight, metabolic pathways are altered along with the BPs associated with cellular stress, including response to heat, response to ROS, ROS metabolic process, and cellular homeostasis, thus indicating increased cellular stress (Figure 5A). We see significant upregulation of heat shock proteins (HSPs)

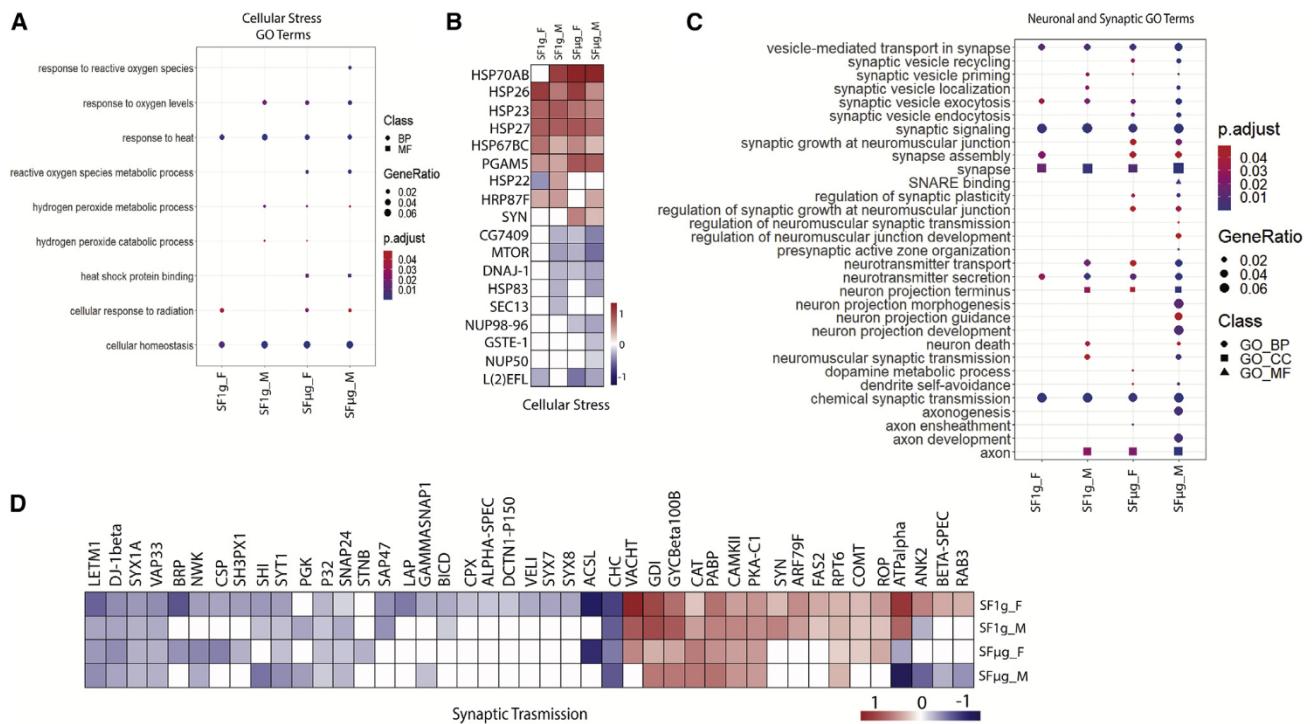


**Figure 5. Increased cellular stress affects neuronal signaling in spaceflight**

(A) Dot plot showing enriched GO terms (adj. p < 0.05) associated with cellular stress in biological processes and molecular function for SF1g and SF $\mu$ g (DEPs) compared with Earth.

(B) Heatmap representation of differential expression (log<sub>2</sub>[fold change]) of significantly altered (adj. p < 0.05) cellular stress response proteins.

(C) Dot plot highlighting enriched GO terms (p < 0.05) associated with neuronal and synaptic signaling in biological processes, molecular function, and cellular components across all conditions (DEPs).

(D) Heatmap displays log<sub>2</sub>[fold change] of proteins that are significantly altered (adj. p < 0.05) in synaptic transmission. For dot plot, the color of the dot represents the adj. p value, and the size represents gene ratio. For the heatmap, the red color represents upregulated and blue shows downregulated proteins.

HSP70AB, HSP26, HSP23, HSP27, and HSP67BC in both spaceflight conditions (Figure 5B). HSPs are the molecular chaperones with cytoprotective properties that are induced in response to a variety of cellular insults, such as heat, radiation, oxidative stress, and altered gravity, to confer protection against deteriorating effects of ROS (Bukau et al., 2006; Hateley et al., 2016; Hosamani et al., 2016; Ikwegbue et al., 2018). Low amounts of ROS aid in neuronal development and function, but excessive ROS levels induced by oxidative stress lead to cellular damage, increased blood-brain barrier permeability, and altered brain morphology, causing neuroinflammation and neuronal death (Gu, 2011). Our observations of increased neuronal loss, apoptosis, and oxidative damage in the fly brain further confirm the effects of oxidative stress during spaceflight (Figure 2). These morphological defects in the brain correlate with the altered expression of proteins that are enriched in functions such as neuronal projection, neuron death, axonogenesis, and synaptic transmission in SF $\mu$ g compared with Earth flies (Figure 5C).

In terms of neuronal functioning, we observed modulations in proteins involved in synaptic transmission across all spaceflight conditions (Figure 5D). For instance, SNARE protein syntaxin 1A (SYX1A), syntaxin binding protein SNAP24, presynaptic calcium sensor synaptotagmin (SYT), presynaptic calcium signaling protein P32, endocytic fission protein dynamin (SHI), and endocytic

coat protein clathrin heavy chain (CHC) are downregulated. Meanwhile, the vesicle-mediated transport protein GDI, an NSF1 protein that aids in disassembly of SNARE complex (COMT), cell-cell adhesion mediator protein FAS2, vesicular trafficking protein ARF79F, and synapsin (SYN), a phosphoprotein associated with synaptic vesicles, among others, are upregulated. These proteins collectively encompass almost every step of the synaptic vesicle cycle. The number of proteins altered is higher in the SF $\mu$ g condition than in the SF1g, and within the SF $\mu$ g condition, males show more changes than females, further reinforcing the selective sensitivity toward males and a dose-dependent response across spaceflight conditions. Additionally, proteins associated with muscle and cytoskeleton are also noted in spaceflight flies (SF $\mu$ g > SF1g) (Figures S5C and S5D), consistent with previous spaceflight findings (Ogneva et al., 2016; Walls et al., 2020).

#### Persistent effects of exposure to spaceflight

Proteomics analysis suggests enrichment of behavioral and aging markers in SF1g and SF $\mu$ g flies (Figure S6A). Specifically, the upregulation of HSP26, HSP27, HSP68, MTPalpha, CAT, SM, TRXR-1, and LDH and the downregulation of DJ-1beta, MSRA, and LEVY are observed across all conditions (Figure S6B). These proteins are also associated with the oxidative stress response,

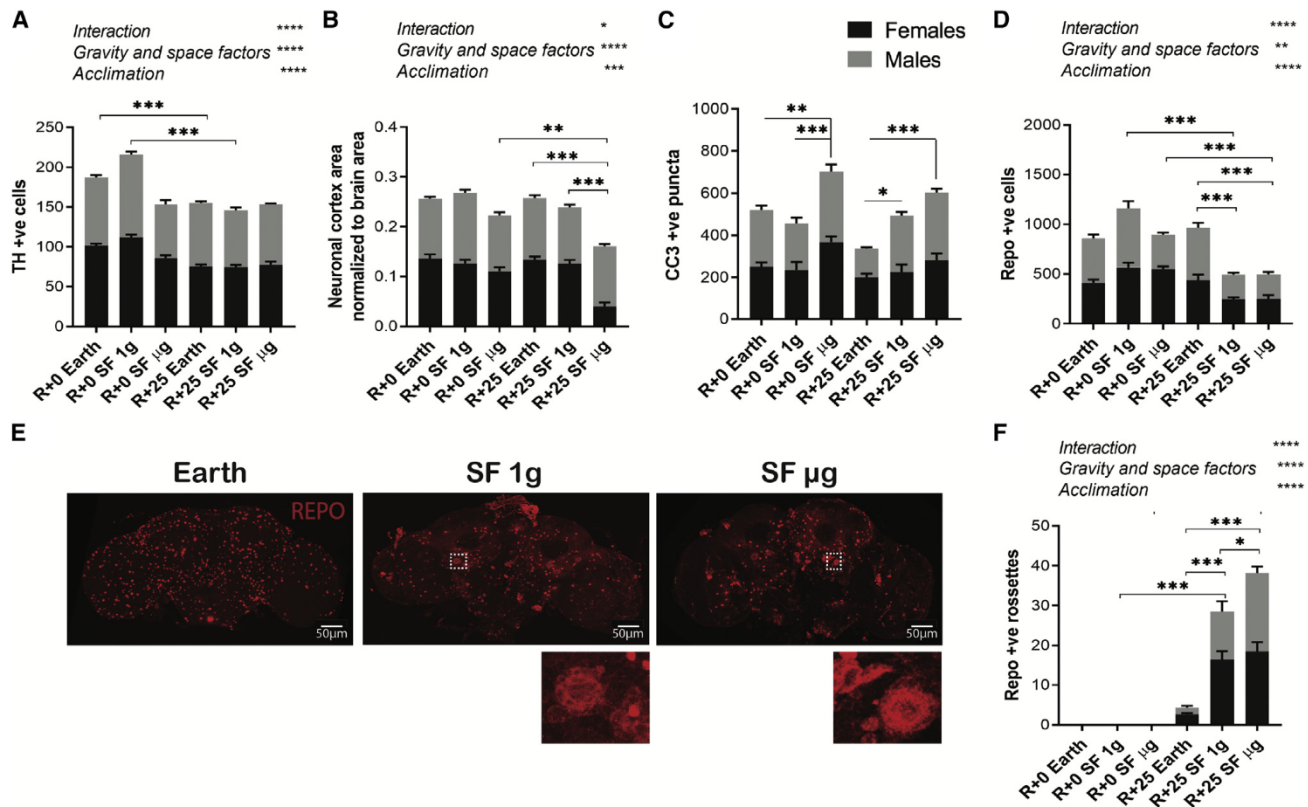


**Figure 6. Persistent effects of spaceflight**

(A–D) Stacked bar plots showing quantification of DA neurons (A) ( $n = 5–10$ ), neuronal cortex area (B) ( $n = 10–14$ ), apoptosis (C) ( $n = 5–7$ ), and glia (D) at R+0 and R+25 days.

(E) Representative images of R+25 fly brains labeled with anti-repo (red). Quantification of repo-positive cells at R+25 days showed total glial loss (D) and increase in the aggregates/rosettes (F) (white box in E inset) in SF $\mu$ g and SF1g ( $n = 6–9$ ). Two-way ANOVA results are displayed above the stacked bar plots. Significance calculated by post-hoc test is represented as \* $p < 0.05$ ; \*\* $p < 0.01$ ; \*\*\* $p < 0.001$ . Scale bar represents 50 microns. Error bars represents SEM.

which has been shown to increase with age (Lavara-Culebras and Paricio, 2007; Liao et al., 2008; Long et al., 2020; Ren et al., 2017). To further understand the effects of spaceflight as the flies acclimate to Earth’s gravity, we aged the flies for 25 days postreturn under terrestrial conditions (R+25 days). Figure S7 shows the observed changes at the R+25 time point for DA neuron counts, neuronal cortex area, apoptosis, and glial phenotypes. Overall, at the R+25 time point, the brain morphology of SF1g and SF $\mu$ g is altered compared with Earth controls, with sex-specific changes observed in the neuronal cortex area (Figure S7). We then performed the longitudinal comparison of morphological changes in fly brains between the R+0 (11–17 days old) and R+25 (36–42 days old) time points. This paradigm is similar to the postmission evaluation of astronauts as they acclimate to Earth conditions over a period of time. Significant reduction of DA neurons was observed early in SF $\mu$ g flies at the R+0 time point compared with the gradual loss of these neurons in Earth and SF1g flies at the R+25 time point (Figure 6A). Typically, terrestrial conditions have not been associated with age-related loss of DA neurons (White et al., 2010); however, the elevated levels of CO<sub>2</sub> in Earth flies (analogous to SF1g and SF $\mu$ g) in this study may contribute to the observed loss of DA neurons as the flies age in the Earth control. Further, comparison of neuronal cortex areas

between R+0 and R+25 data showed no change in the Earth flies, while a decreasing trend over time was noted in SF1g flies and a significant reduction in SF $\mu$ g flies, thus suggesting increased neuronal loss with age in space-reared flies (Figure 6B). This loss correlates with increased apoptosis observed in R+25 flies, both SF1g (39%) and SF $\mu$ g (70%), compared with R+25 Earth flies (Figure 6C). This progressive increase in apoptosis in space-reared flies (R+25 Earth < R+25 SF1g < R+25 SF $\mu$ g) may suggest a dose-dependent response in flies as we move from Earth to space conditions with exposure to multiple stressors, including increased ionizing radiation combined with exposure to reduced gravity.

Additionally, we assessed glia, the primary phagocytic cell in the CNS that are required to clear neuronal debris induced by oxidative stress (Bilimoria and Stevens, 2015; Casano and Peri, 2015; Cronk and Kipnis, 2013; Cunningham, 2013; Freeman, 2006; Hanisch and Kettenmann, 2007). At R+25, while we observe a slight, but non-significant, increase in glial cell numbers under Earth conditions (females: 7%, males: 17%), a significant depletion of the glial population in Earth-acclimated SF1g (females: 56%, males: 59%) and a sex-specific depletion in SF $\mu$ g flies (females: 54%, males: 33%) are noted compared with their respective R+0 time point (Figures 6D and 6E). This

depletion of the glial population can be due to burdening of the clearance system, eventually leading to glial apoptosis (Block et al., 2007), but additional investigation is warranted. Furthermore, as the flies age, we observe aggregates of glial cells that resemble rosettes (Figure 6E, inset). These rosettes were distinct in size and appearance from other glial cells and were not counted toward total repo-positive cell counts (Figure 6D); instead, they were counted separately (Figure 6F). This rosette phenotype is absent at the R+0 time point in all conditions, whereas it is observed at the R+25 time point specifically after exposure to spaceflight-related stressors in a dose-dependent manner (R+25 Earth < R+25 SF1g < R+25 SF $\mu$ g) (Figure 6F). We believe the rosette to be a phenotype manifested as a long-term effect of the spaceflight environment. The rosette formation could result from factors such as elevated CO<sub>2</sub> levels and could be exacerbated by the combinatorial effect of other spaceflight stressors such as ionizing radiation and reduced gravity.

While some of the immunohistochemical and omics results described here resemble early aging, more assays at additional time points need to be performed for further validation of the effect of spaceflight on related aging phenotypes. Although omics profiling at the R+25 time point would be informative and will be considered in future missions, these experiments were not feasible here since the flies were distributed for the other assays reported above. Taken together, the brain morphology at the R+0 time point is similar in SF1g and Earth conditions, but as the flies age postflight under terrestrial conditions, the morphological deficits start manifesting in SF1g flies and are worsened over time in SF $\mu$ g flies, suggesting a phenotype that is manifested after exposure to spaceflight.

## DISCUSSION

Deep-space exploration will expose space travelers to several environmental challenges, thereby altering the homeostatic equilibrium of various physiological systems, including the CNS. Understanding the risks to the CNS and identifying countermeasures to mitigate these risks in astronauts will be crucial to ensure the success of missions to the Moon and Mars. Using MVP, a fruit fly space habitat, we provide insights into spaceflight effects on the brain at the molecular, morphological, and behavioral levels. While AG by rotation of the spacecraft is being considered as a potential countermeasure to  $\mu$ g, there is a gap in our understanding of AG prescriptions required to ameliorate the health concerns during spaceflight (Clément, 2017; Clément and Traon, 2004; Mao et al., 2018a; Young, 1999). To address this knowledge gap, we utilized the MVP hardware featuring an inflight centrifuge that simulates Earth's gravity on the ISS (SF1g). SF1g served two objectives: (1) assessment of the use of AG as a countermeasure and (2) distinguishing the effects of  $\mu$ g from other spaceflight stressors, such as radiation.

A key feature of the MVP hardware, the inflight video-recording capability, aided in assessing the health of the flies during the mission and provided real-time data of behavioral alterations caused by the change in the gravitational environment. Due to the large number of videos taken on the mission, manual analysis by visual assessment was not feasible nor was the use of specialized equipment traditionally used to assess fly behavior

in ground laboratories (Chan et al., 2012; Inan et al., 2009, 2011; Kohlhoff et al., 2011; Slawson et al., 2009). Also, the constraints in video quality, such as uneven light distribution and the inability to focus on flies in the foreground and the background, prevented the use of sophisticated tracking and machine-learning algorithms for behavioral analysis. Therefore, a simple yet effective automated method was developed to quantitatively capture overall behavioral differences across spaceflight conditions. The overall level of activity of a population is a trait influenced by the environment and can be used to assess other physiological changes. Miller et al. suggested that fly hyperactivity in  $\mu$ g is a result of their innate negative geotactic response (Miller et al., 2002). Interestingly, our findings follow a similar trend, apart from the population flux point (day 20), we consistently observed that flies in SF $\mu$ g are more active than those in SF1g (Figures 1D and 1E). These data suggest that AG may suppress the hyperactive behavior in flies during spaceflight. Similar increases in fly activity (Benguría et al., 1996) and mouse circling behavior (Ronca et al., 2019) in spaceflight conditions have been reported. Future improvements in the flight hardware might aid in quantifying individual fly activity, thus providing further insights into behavioral changes caused by gravity changes and the ability to test the effectiveness of countermeasures.

A substantial fraction of the literature on the CNS effects of spaceflight focuses on either anatomical changes or molecular changes using omics platforms. In this study, we took a multimodal approach combining the morphological analysis with the omics-based molecular phenotyping for a comprehensive understanding of the underlying mechanisms associated with spaceflight-induced brain changes. At the transcriptomics level, we observed a higher number of differentially regulated genes in SF $\mu$ g compared with Earth, specifically in females. Meanwhile, the SF1g females show fewer changes in RNA compared with Earth (Figure 3). Interestingly, at the proteomic level, the number of DEPs is relatively similar and shows considerable overlap across spaceflight conditions (SF1g versus Earth and SF $\mu$ g versus Earth). In many studies, a discordance is observed between the two omics platforms; nevertheless, each dataset offers unique insights into spaceflight-associated changes (Casas-Vila et al., 2017; De Sousa Abreu et al., 2009). While transcriptomic analyses provide broad-scale insights into molecular dynamics that occur on the level of mRNA regulation, most physiological processes are driven by protein function. Based on proteomics, one important theme that was captured across both spaceflight conditions was a change in metabolic pathways, including oxidative phosphorylation (Figures 3, 4, and 5). These are consistent with previously published data on space-flown human kidney cells (Hammond et al., 2000) and mouse brain subjected to spaceflight (Mao et al., 2018b).

The brain is a metabolically dynamic and high-energy-demanding organ that is dependent on mitochondria for deriving energy via various metabolic processes that converge at glycolysis and oxidative phosphorylation (Hall et al., 2012; Magistretti and Allaman, 2015). Normal functioning of the brain requires a tight temporal and spatial regulation of metabolite supply for energy production (Roy and Sherrington, 1890; Watts et al., 2018). We observe such metabolic regulation in spaceflight flies with increased glucose, fatty acid, and amino acid metabolism

(Figures 4E, 4H, and 4I). Additionally, spaceflight flies exhibit alteration in proteins of the ETC and ATP metabolism (Figures 4F and 4G), similar to the observations in mice, astronauts, and the NASA Twins Study (da Silveira et al., 2020). Such dysregulation of ETC and abnormal mitochondrial dynamics (Figure 4D) can lead to mitochondrial and oxidative stress via ROS production (Bhatti et al., 2017). Oxidative stress during spaceflight is further evidenced by an increase in 8-oxo-dG, a cellular oxidative stress marker, in the SF $\mu$ g fly brain at the R+0 time point (Figures 2E and 2I) and is consistent with the increase of 8-oxo-dG in urine and plasma samples in astronauts (Rai et al., 2011; da Silveira et al., 2020). On the contrary, SF1g brains at the R+0 time point showed no significant change in the 8-oxo-dG marker, thus suggesting that AG can suppress oxidative damage in the brain immediately after return from spaceflight (Figures 2E and 2I).

We hypothesize that the observed alterations in the metabolic pathways are an effort to restore cellular homeostasis via metabolic reprogramming. While homeostasis is restored in R+0 SF1g, possibly due to AG, as evidenced by their similar brain morphology to Earth flies (Figure 2),  $\mu$ g in SF $\mu$ g acts as an additional stressor, potentially resulting in elevated oxidative stress. This stress can further trigger a cascade of events leading to neuronal damage as noted in the behavioral deficits (Figure 2A), loss of DA neurons (Figures 2E and 2F), decreased neuronal cortex and neuropil areas (Figures 2B–2D and S3B), and increased apoptosis (Figures 2E and 2H) in SF $\mu$ g flies. Additionally, we observe perturbations in synaptic transmission proteins during spaceflight (Figures 5C and 5D), which, in combination with bioenergetic changes (Figure 4), can result in dysregulation of calcium homeostasis and synaptic degeneration (Mattson and Liu, 2002). Synaptic changes have also been documented in multiple spaceflight and ground-based rodent studies (Bondar, 2005; DeFelipe et al., 2002; Gaofei et al., 2009; Howe et al., 2019; Machida et al., 2010; Parihar et al., 2015, 2016; Ranjan et al., 2014; Ross and Varelas, 2005; Sokolova et al., 2015; Wang et al., 2015). Neuronal damage and loss induced by elevated oxidative stress can potentially alter the glial response, initiating phagocytosis to clear neuronal debris (Block et al., 2007). While our observations of glial numbers immediately after return (R+0) show an increasing trend in SF $\mu$ g females and SF1g (both females and males) (Figure 2G), further analysis is warranted to elucidate the underlying mechanism of change in glial function. Collectively, our observations suggest that brain morphological changes due to spaceflight-induced oxidative stress are more pronounced in  $\mu$ g conditions, and AG can provide partial protection to these phenotypes.

Based on our omics data, R+0 morphology, and the radiation levels on the ISS, gravity seems to have a significant impact on the immediate phenotypes of spaceflight with larger observable changes in SF $\mu$ g compared with SF1g. The environment experienced by the flies in SF $\mu$ g compared with SF1g allows the comparison of gravity separately from the combined effect of the other spaceflight stressors like radiation, elevated CO<sub>2</sub>, and sound pressure, which would equally impact both SF1g and SF $\mu$ g. Although the morphological manifestations are not observed in SF1g flies at the R+0 time point, with age (R+25), the phenotypes progressively present themselves in the form of increased apoptosis, neuronal loss, glial loss, and aggregate

formation (Figures 6A–6F). Glial loss may be attributed to the relocation of glia to the neuronal debris, thus resulting in aggregates (formation of rosettes), a phenotype specific to the spaceflight environment. These phenotypes in SF1g at R+25 may be a delayed response to radiation combined with exposure to other space stressors such as elevated CO<sub>2</sub>. Radiation studies in ground-based rodent models indicate that exposure to deep-space radiation (galactic cosmic radiation [GCR]) alone can affect behavior (Dutta et al., 2018; Euston et al., 2012; Parihar et al., 2015, 2018; Raber et al., 2018) and neuronal phenotypes (Davis et al., 2015; Howe et al., 2019; Impey et al., 2016; Krukowski et al., 2018; Parihar et al., 2015, 2016; Raber et al., 2016, 2018, 2019; Rabin et al., 2014; Whoolery et al., 2017). In an enclosed and isolated environment of the ISS, astronauts experience elevated CO<sub>2</sub> levels that are considerably higher than ambient levels on Earth (Mahadevan et al., 2021). In our study, the Earth control flies were exposed to an environment mimicking the ISS and experienced high CO<sub>2</sub> levels similar to SF1g and SF $\mu$ g flies, in contrast to regular lab conditions. Mild chronic hypercapnia due to constant exposure of elevated CO<sub>2</sub> levels may contribute to the observed deficits of decreased TH-positive cells and repo-positive rosettes (<10) in the Earth control flies at R+25, along with the increased cell death (CC3-positive cells) and DNA oxidation (8-oxo-dG-positive cells) as noted at R+0 in Earth controls. In fact, in our ground-based study, we observed minimal cell death and DNA oxidation under normal terrestrial CO<sub>2</sub> levels compared with Earth control brains from the MVP mission exposed to elevated CO<sub>2</sub> levels (data not shown). Thus, the observations reported in the Earth controls are part of the unique spaceflight paradigm and may not be comparable to controls in terrestrial studies. While ground studies are important in separating the effects of individual space stressors, spaceflight studies are particularly relevant as we prepare for long-duration human missions to the Moon and Mars, where there will be a combination of exposures to reduced gravity and doses of ionizing radiation that will be higher than in LEO (Mao et al., 2017; Straume et al., 2017).

This study integrates transcriptomic, proteomic, morphological, and behavioral analyses to investigate the effects of spaceflight on *Drosophila* CNS both during and after return from spaceflight. Further, our study utilizes inflight centrifuge mimicking Earth 1g as a control that allowed us to separate  $\mu$ g from the effects of other spaceflight environmental factors such as ionizing radiation. Additionally, the postflight acclimation to Earth's conditions is relevant to understanding the sustained effects of spaceflight on the CNS. Our integrated approach suggests that oxidative stress during spaceflight leads to differential regulation of metabolic pathways, oxidative phosphorylation, and synaptic transmission resulting in neuronal deficits, glial changes, increased apoptosis, and behavioral impairments in *Drosophila*. Furthermore, this study indicates that  $\mu$ g is an important, but not an exclusive, environmental factor contributing to the neurobehavioral outcomes during long-term deep-space missions. AG may provide a measure for short-term protection, but long-term solutions still need to be explored, especially for long-duration missions in deep space. Earth's magnetosphere partially protects against ionizing radiation from GCRs and solar particle events (SPEs) in LEO, but beyond LEO, deep-space irradiation

will pose significant risks to crew member health. Thus, along with AG, future countermeasure studies should target these pathways in model organisms that are amenable to large-scale screening in space.

### Limitations of the study

The opportunity to conduct spaceflight experiments is not only rare and expensive, but the logistical constraints of such studies also make them highly challenging to perform (Inokuchi et al., 2007; Rutter et al., 2020). For instance, the experiment launch and retrieval can be significantly altered due to weather or technical issues with the spacecraft, thus necessitating a flexible experimental design to achieve the intended science goals. In fact, our sample return was delayed from 31 days to 34 days due to weather-related issues. Another constraint of spaceflight studies is that retrieving exact age-matched flies is often not feasible. Some of the previous spaceflight studies have been conducted on mixed-age populations of flies from different generations (depending on the mission's timeline). But with the MVP hardware, the astronauts could accommodate multiple timed inflight operations, including a 5.5-day egg-lay period (Figure S1C), thus ensuring that the retrieved flies were from the same generation and within a relatively close age range (11–17 days). Our strategy of testing randomly selected flies from this collection ensured that the average ages were similar and allowed for an unbiased comparison across groups of flies. Further, spaceflight experiments are severely limited by mass and volume. Therefore, the number of samples retrieved is limited by the capacity of the flight hardware. In this experiment, a large population of live flies were retrieved from the MVP hardware, allowing us to conduct the presented experiments. Additional flies would have allowed for longitudinal multi-omics profiling at the R+25 time point but were unavailable for this experiment. The current study, MVP-FLY-01 mission, was an important one-time validation flight for the MVP hardware to demonstrate its ability to support *Drosophila* research on the ISS. After its successful validation, as demonstrated by this experiment, this hardware will form the framework for multiple *Drosophila* spaceflight investigations in the future.

### STAR★METHODS

Detailed methods are provided in the online version of this paper and include the following:

- **KEY RESOURCES TABLE**
- **RESOURCE AVAILABILITY**
  - Lead contact
  - Materials availability
  - Data and code availability
- **EXPERIMENTAL MODEL AND SUBJECT DETAILS**
  - Spaceflight mission and hardware description
  - Fly husbandry, loading the module, and development
- **METHOD DETAILS**
  - Inflight behavioral analysis
  - Climbing assay
  - Immunohistochemistry and confocal imaging of brains

- RNA isolation, sequencing, and analysis of fly heads
- Proteomics and analysis of fly heads
- Gene ontology and KEGG analysis

- **QUANTIFICATION AND STATISTICAL ANALYSIS**

### SUPPLEMENTAL INFORMATION

Supplemental information can be found online at <https://doi.org/10.1016/j.celrep.2022.111279>.

### ACKNOWLEDGMENTS

We would like to thank the ISS Research Integration Office at NASA JSC for funding to S.B. for the validation of the MVP platform (NASA-OZ [2017–2018]). The Nevada Proteomics and Bioinformatics Centers are supported by a grant from the National Institute of General Medical Sciences (GM103440). Bioinformatics is also supported by 5 U54 GM104944. We would like to thank Redwire (previously Techshot, Inc.) for supporting the mission and developing the hardware used. We gratefully acknowledge assistance from C. Cheung, P. Bhavsar, E. Pane, C. Angadi, E. Cekanaviciute, I. Fernandes, and M. Torres. We thank Dr. Alwood and Dr. Govind for careful reading of the manuscript. We would like to thank the flight crew for technical assistance aboard the ISS.

### AUTHOR CONTRIBUTIONS

Conceptualization, S.B., S.D.M., and J.I.; methodology, S.D.M., J.I., and R.G.; software, R.M.D.-B., S.V.C., J.P., A.T., M.J., and S.G.; formal analysis, S.D.M., J.I., A.P., A.T., M.J., J.P., D.R.Q., and R.J.W.; data curation, A.T., J.P., D.R.Q., and R.J.W.; writing—original draft, S.D.M. and J.I.; writing—review & editing, S.B., S.D.M., J.I., S.G., S.V.C., S.A., and M.B.S.; funding acquisition, S.B.; supervision, S.B.

### DECLARATION OF INTERESTS

The authors declare no competing interests.

### INCLUSION AND DIVERSITY

We worked to ensure sex balance in the selection of non-human subjects. One or more of the authors of this paper self-identifies as an underrepresented ethnic minority in science.

Received: July 26, 2021  
Revised: March 16, 2022  
Accepted: August 5, 2022  
Published: September 6, 2022

### REFERENCES

- Afshinnekoo, E., Scott, R.T., MacKay, M.J., Pariset, E., Cekanaviciute, E., Barker, R., Gilroy, S., Hassane, D., Smith, S.M., Zwart, S.R., et al. (2020). Fundamental biological features of spaceflight: advancing the field to enable deep-space exploration. *Cell* 183, 1162–1184.
- Benguría, A., Grande, E., De Juan, E., Ugalde, C., Miquel, J., Garesse, R., and Marco, R. (1996). Microgravity effects on *Drosophila melanogaster* behavior and aging. Implications of the IML-2 experiment. *J. Biotechnol.* 47, 191–201.
- Bhatti, J.S., Bhatti, G.K., and Reddy, P.H. (2017). Mitochondrial dysfunction and oxidative stress in metabolic disorders — a step towards mitochondria based therapeutic strategies. *Biochim. Biophys. Acta Mol. Basis Dis.* 1863, 1066–1077.
- Bilimoria, P.M., and Stevens, B. (2015). Microglia function during brain development: new insights from animal models. *Brain Res.* 1617, 7–17.
- Block, M.L., Zecca, L., and Hong, J.S. (2007). Microglia-mediated neurotoxicity: uncovering the molecular mechanisms. *Nat. Rev. Neurosci.* 8, 57–69.

- Bondar, R.L. (2005). The Neurolab Spacelab Mission: Neuroscience Research in Space: Results from the STS-90 (Neurolab Spacelab Mission).
- Robey, R.B., Weisz, J., Kuemmerle, N.B., Salzberg, A.C., Berg, A., Brown, D.G., Kubik, L., Palorini, R., Al-Mulla, F., Al-Temaimi, R., et al. (2015). Metabolic reprogramming and dysregulated metabolism: cause, consequence and/or enabler of environmental carcinogenesis? *Carcinogenesis* 36, S203–S231.
- Bukau, B., Weissman, J., and Horwich, A. (2006). Molecular chaperones and protein quality control. *Cell* 125, 443–451.
- Carbon, S., Douglass, E., Good, B.M., Unni, D.R., Harris, N.L., Mungall, C.J., Basu, S., Chisholm, R.L., Dodson, R.J., Hartline, E., Fey, P., et al.; Gene Ontology Consortium (2021). The gene ontology resource: enriching a GOld mine. *Nucleic Acids Res.* 49, D325–D334.
- Casano, A.M., and Peri, F. (2015). Microglia: multitasking specialists of the brain. *Dev. Cell* 32, 469–477.
- Casas-Vila, N., Bluhm, A., Sayols, S., Dinges, N., Dejung, M., Altenhein, T., Kappeli, D., Altenhein, B., Roignant, J.Y., and Butter, F. (2017). The developmental proteome of *Drosophila melanogaster*. *Genome Res.* 27, 1273–1285.
- Cekanaviciute, E., Rosi, S., and Costes, S.V. (2018). Central nervous system responses to simulated galactic cosmic rays. *Int. J. Mol. Sci.* 19, 36699.
- Chakraborty, R., Vepuri, V., Mhatre, S.D., Paddock, B.E., Miller, S., Michelson, S.J., Delvadia, R., Desai, A., Vinokur, M., Melicharek, D.J., et al. (2011). Characterization of a *Drosophila* Alzheimer's disease model: pharmacological rescue of cognitive defects. *PLoS One* 6, e20799.
- Chan, K.L., Inan, O., Bhattacharya, S., and Marcu, O. (2012). Estimating the speed of *Drosophila* locomotion using an automated behavior detection and analysis system. *Fly* 6, 205–210.
- Clément, G., and Pavy-Le Traon, A. (2004). Centrifugation as a countermeasure during actual and simulated microgravity: a review. *Eur. J. Appl. Physiol.* 92, 235–248.
- Clément, G. (2017). International roadmap for artificial gravity research. *NPJ Microgravity* 3, 29.
- Clément, G.R., Boyle, R.D., George, K.A., Nelson, G.A., Reschke, M.F., Williams, T.J., and Paloski, W.H. (2020). Challenges to the central nervous system during human spaceflight missions to Mars. *J. Neurophysiol.* 123, 2037–2063.
- Cronk, J.C., and Kipnis, J. (2013). Microglia - the brain's busy bees. *F1000Prime Rep.* 5, 53.
- Crucian, B., Stowe, R.P., Mehta, S., Quiariarte, H., Pierson, D., and Sams, C. (2015). Alterations in adaptive immunity persist during long-duration spaceflight. *NPJ Microgravity* 1, 15013.
- Cunningham, C. (2013). Microglia and neurodegeneration: the role of systemic inflammation. *Glia* 61, 71–90.
- da Silveira, W.A., Fazelinia, H., Rosenthal, S.B., Laiakis, E.C., Kim, M.S., Meydan, C., Kidane, Y., Rathi, K.S., Smith, S.M., Stear, B., et al. (2020). Comprehensive multi-omics analysis reveals mitochondrial stress as a central biological hub for spaceflight impact. *Cell* 183, 1185–1201.e20.
- Davis, C.M., DeCicco-Skinner, K.L., and Hienz, R.D. (2015). Deficits in sustained attention and changes in dopaminergic protein levels following exposure to proton radiation are related to basal dopaminergic function. *PLoS One* 10, e0144556.
- de Luca, C., Deeva, I., Mariani, S., Maiani, G., Stancato, A., and Korkina, L. (2009). Monitoring antioxidant defenses and free radical production in space-flight, aviation and railway engine operators, for the prevention and treatment of oxidative stress, immunological impairment, and pre-mature cell aging. *Toxicol. Ind. Health* 25, 259–267.
- De Sousa Abreu, R., Penalva, L.O., Marcotte, E.M., and Vogel, C. (2009). Global signatures of protein and mRNA expression levels. *Mol. Biosyst.* 5, 1512–1526.
- DeFelipe, J., Arellano, J.I., Merchán-Pérez, A., González-Albo, M.C., Walton, K., and Linás, R. (2002). Spaceflight induces changes in the synaptic circuitry of the postnatal developing neocortex. *Cereb. Cortex* 12, 883–891.
- Dobin, A., Davis, C.A., Schlesinger, F., Drenkow, J., Zaleski, C., Jha, S., Batut, P., Chaisson, M., and Gingeras, T.R. (2013). STAR: ultrafast universal RNA-seq aligner. *Bioinformatics* 29, 15–21.
- Dutta, S.M., Hadley, M.M., Peterman, S., Jewell, J.S., Duncan, V.D., and Britten, R.A. (2018). Quantitative proteomic analysis of the Hippocampus of rats with GCR-induced spatial memory impairment. *Radiat. Res.* 189, 136–145.
- Euston, D.R., Gruber, A.J., and McNaughton, B.L. (2012). The role of medial prefrontal cortex in memory and decision making. *Neuron* 76, 1057–1070.
- Feany, M.B., and Bender, W.W. (2000). A *Drosophila* model of Parkinson's disease. *Nature* 404, 394–398.
- Fernández-Moreno, M.A., Farr, C.L., Kaguni, L.S., and Garesse, R. (2007). *Drosophila melanogaster* as a model system to study mitochondrial biology. *Methods Mol. Biol.* 372, 33–49.
- Freeman, M.R. (2006). Sculpting the nervous system: glial control of neuronal development. *Curr. Opin. Neurobiol.* 16, 119–125.
- Friedman, J. (2011). Why is the nervous system vulnerable to oxidative stress? In *Oxidative Stress and Free Radical Damage in Neurology* (Humana Press), pp. 19–27.
- Gaofei, H., Ying, M., Yun, Z., De, C., Shengyuan, X., and Yulin, D. (2009). SNAREs-related pathways in rat brains under simulated microgravity environment. In *3rd Int. Conf. Bioinforma. Biomed. Eng. ICBBE*, 18, pp. 1–4.
- Garrett-Bakelman, F.E., Darshi, M., Green, S.J., Gur, R.C., Lin, L., Macias, B.R., McKenna, M.J., Meydan, C., Mishra, T., Nasrini, J., et al. (2019). The NASA twins study: a multidimensional analysis of a year-long human spaceflight. *Science* 364, eaau8650.
- Gilbert, R., Torres, M., Clemens, R., Hateley, S., Hosamani, R., Wade, W., and Bhattacharya, S. (2020). Spaceflight and simulated microgravity conditions increase virulence of *Serratia marcescens* in the *Drosophila melanogaster* infection model. *NPJ Microgravity* 6, 4–9.
- Grimm, D., Grosse, J., Wehland, M., Mann, V., Reseland, J.E., Sundaresan, A., and Corydon, T.J. (2016). The impact of microgravity on bone in humans. *Bone* 87, 44–56.
- Gu, Y., Dee, C.M., and Shen, J. (2011). Interaction of free radicals, matrix metalloproteinases and caveolin-1 impacts blood-brain barrier permeability. *Front. Biosci. Front. Biosci.* 3, 1216–1231.
- Hall, C.N., Klein-Flügge, M.C., Howarth, C., and Attwell, D. (2012). Oxidative phosphorylation, not glycolysis, powers presynaptic and postsynaptic mechanisms underlying brain information processing. *J. Neurosci.* 32, 8940–8951.
- Hammond, T.G., Benes, E., O'Reilly, K.C., Wolf, D.A., Linnehan, R.M., Taher, A., Kaysen, J.H., Allen, P.L., and Goodwin, T.J. (2000). Mechanical culture conditions effect gene expression: gravity-induced changes on the space shuttle. *Physiol. Genomics* 3, 163–173.
- Hanisch, U.K., and Kettenmann, H. (2007). Microglia: active sensor and versatile effector cells in the normal and pathologic brain. *Nat. Neurosci.* 10, 1387–1394.
- Hateley, S., Hosamani, R., Bhardwaj, S.R., Pachter, L., and Bhattacharya, S. (2016). Transcriptomic response of *Drosophila melanogaster* pupae developed in hypergravity. *Genomics* 108, 158–167.
- Horie, K., Kato, T., Kudo, T., Sasanuma, H., Miyauchi, M., Akiyama, N., Miyao, T., Seki, T., Ishikawa, T., Takakura, Y., et al. (2019). Impact of spaceflight on the murine thymus and mitigation by exposure to artificial gravity during spaceflight. *Sci. Rep.* 9, 19866.
- Hosamani, R., Leib, R., Bhardwaj, S.R., Adams, C.M., and Bhattacharya, S. (2016). Elucidating the “gravome”: quantitative proteomic profiling of the response to chronic hypergravity in *Drosophila*. *J. Proteome Res.* 15, 4165–4175.
- Howe, A., Kiffer, F., Alexander, T.C., Sridharan, V., Wang, J., Ntagwabira, F., Rodriguez, A., Boerma, M., and Allen, A.R. (2019). Long-term changes in cognition and physiology after low-dose 160 irradiation. *Int. J. Mol. Sci.* 20, E188.
- Hussin, M., Ismail, M.R., and Ahmad, M.S. (2017). Air-conditioned university laboratories: comparing CO2 measurement for centralized and split-unit systems. *Journal of King Saud University - Engineering Sciences* 29, 191–201.



- Iijima, K., Liu, H.P., Chiang, A.S., Hearn, S.A., Konsolaki, M., and Zhong, Y. (2004). Dissecting the pathological effects of human A $\beta$ 40 and A $\beta$ 42 in *Drosophila*: a potential model for Alzheimer's disease. *Proc. Natl. Acad. Sci. USA* *101*, 6623–6628.
- Ikenaga, M., Yoshikawa, I., Kojo, M., Ayaki, T., Ryo, H., Ishizaki, K., Kato, T., Yamamoto, H., and Hara, R. (1997). Mutations induced in *Drosophila* during space flight. *Biol. Sci. Space* *11*, 346–350.
- Ikwegbue, P.C., Masamba, P., Oyinloye, B.E., and Kappo, A.P. (2018). Roles of heat shock proteins in apoptosis, oxidative stress, human inflammatory diseases, and cancer. *Pharmaceuticals* *11*.
- Impey, S., Jopson, T., Pelz, C., Tafessu, A., Fareh, F., Zuloaga, D., Marzulla, T., Riparip, L.K., Stewart, B., Rosi, S., et al. (2016). Short- and long-term effects of 56Fe irradiation on cognition and hippocampal DNA methylation and gene expression. *BMC Genom.* *17*, 825.
- Inan, O.T., Etemadi, M., Sanchez, M.E., Marcu, O., Bhattacharya, S., and Kovacs, G.T.A. (2009). A miniaturized video system for monitoring the locomotor activity of walking *Drosophila melanogaster* in space and terrestrial settings. *IEEE Trans. Biomed. Eng.* *56*, 522–524.
- Inan, O.T., Marcu, O., Sanchez, M.E., Bhattacharya, S., and Kovacs, G.T.A. (2011). A portable system for monitoring the behavioral activity of *Drosophila*. *J. Neurosci. Methods* *202*, 45–52.
- Indo, H.P., Majima, H.J., Terada, M., Suenaga, S., Tomita, K., Yamada, S., Higashibata, A., Ishioka, N., Kanekura, T., Nonaka, I., et al. (2016). Changes in mitochondrial homeostasis and redox status in astronauts following long stays in space. *Sci. Rep.* *6*, 39015.
- Inokuchi, H., Fukui, K., Kogure, K., Muneo, T., Kinoshita, K., Izumi, R., and Fujimori, Y. (2007). Planning Guide for Space Experiment Research (Japan Aerospace Exploration Agency Japan Space Forum).
- Iyer, J., Singh, M.D., Jensen, M., Patel, P., Pizzo, L., Huber, E., Koerselman, H., Weiner, A.T., Lepanto, P., Vadodaria, K., et al. (2018). Pervasive genetic interactions modulate neurodevelopmental defects of the autism-associated 16p11.2 deletion in *Drosophila melanogaster*. *Nat. Commun.* *9*, 2548.
- Khan, A., and Mathelier, A. (2017). Intervene: a tool for intersection and visualization of multiple gene or genomic region sets. *BMC Bioinf.* *18*, 287–288.
- Kohlhoff, K.J., Jahn, T.R., Lomas, D.A., Dobson, C.M., Crowther, D.C., and Vendruscolo, M. (2011). The iFly tracking system for an automated locomotor and behavioural analysis of *drosophila melanogaster*. *Integr. Biol.* *3*, 755–760.
- Kolde, R. (2015). Pheatmap: Pretty Heatmaps. <https://github.com/raivokolde/pheatmap>.
- Kononikhin, A.S., Starodubtseva, N.L., Pastushkova, L.K., Kashirina, D.N., Fedorchenko, K.Y., Brhozovsky, A.G., Popov, I.A., Larina, I.M., and Nikolaev, E.N. (2017). Spaceflight induced changes in the human proteome. *Expert Rev. Proteomics* *14*, 15–29.
- Krukowski, K., Feng, X., Paladini, M.S., Chou, A., Sacramento, K., Grue, K., Riparip, L.K., Jones, T., Campbell-Beachler, M., Nelson, G., and Rosi, S. (2018). Temporary microglia-depletion after cosmic radiation modifies phagocytic activity and prevents cognitive deficits. *Sci. Rep.* *8*, 10297.
- Lai Polo, S.H., Saravia-Butler, A.M., Boyko, V., Dinh, M.T., Chen, Y.C., Fogle, H., Reinsch, S.S., Ray, S., Chakravarty, K., Marcu, O., et al. (2020). RNAseq analysis of rodent spaceflight experiments is confounded by sample collection techniques. *iScience* *23*, 101733.
- Lavara-Culebras, E., and Paricio, N. (2007). *Drosophila* DJ-1 mutants are sensitive to oxidative stress and show reduced lifespan and motor deficits. *Gene* *400*, 158–165.
- Liao, P.C., Lin, H.Y., Yuh, C.H., Yu, L.K., and Wang, H.D. (2008). The effect of neuronal expression of heat shock proteins 26 and 27 on lifespan, neurodegeneration, and apoptosis in *Drosophila*. *Biochem. Biophys. Res. Commun.* *376*, 637–641.
- Long, D.M., Frame, A.K., Reardon, P.N., Cumming, R.C., Hendrix, D.A., Kretzschmar, D., and Gieblutowicz, J.M. (2020). Lactate dehydrogenase expression modulates longevity and neurodegeneration in *Drosophila melanogaster*. *Aging (Albany, NY)* *12*, 10041–10058.
- Love, M.I., Huber, W., and Anders, S. (2014). Moderated estimation of fold change and dispersion for RNA-seq data with DESeq2. *Genome Biol.* *15*, 550. <https://doi.org/10.1186/s13059-014-0550-8>.
- Luengo, H.C.L., van Vliet, L.J., Rieger, B., and van Ginkel, M. (1999). DIPImage: A scientific image processing toolbox for MATLAB. Delft: Quantitative Imaging Group. The Netherlands: Delft University of Technology. <https://github.com/DIPIlib/diplib>.
- Lundby, A., Secher, A., Lage, K., Nordsborg, N.B., Dmytriiev, A., Lundby, C., and Olsen, J.V. (2012). Quantitative maps of protein phosphorylation sites across 14 different rat organs and tissues. *Nat. Commun.* *3*, 876.
- Machida, M., Lonart, G., and Britten, R.A. (2010). Low (60 cGy) doses of (56)Fe HZE-particle radiation lead to a persistent reduction in the glutamatergic readily releasable pool in rat hippocampal synaptosomes. *Radiat. Res.* *174*, 618–623.
- Magistretti, P.J., and Allaman, I. (2015). A cellular perspective on brain energy metabolism and functional imaging. *Neuron* *86*, 883–901.
- Mahadevan, A.D., Hupfeld, K.E., Lee, J.K., De Dios, Y.E., Kofman, I.S., Beltran, N.E., Mulder, E., Bloomberg, J.J., Mulavara, A.P., and Seidler, R.D. (2021). Head-down-tilt bed rest with elevated CO<sub>2</sub>: effects of a pilot spaceflight analog on neural function and performance during a cognitive-motor dual task. *Front. Physiol.* *12*, 654906.
- Mao, X.W., Byrum, S., Nishiyama, N.C., Pecaut, M.J., Sridharan, V., Boerma, M., Tackett, A.J., Shiba, D., Shirakawa, M., Takahashi, S., and Delp, M.D. (2018a). Impact of spaceflight and artificial gravity on the mouse retina: biochemical and proteomic analysis. *Int. J. Mol. Sci.* *19*, E2546.
- Mao, X.W., Nishiyama, N.C., Byrum, S.D., Stanbouly, S., Jones, T., Holley, J., Sridharan, V., Boerma, M., Tackett, A.J., Willey, J.S., et al. (2020). Spaceflight induces oxidative damage to blood-brain barrier integrity in a mouse model. *FASEB J* *34*, 15516–15530.
- Mao, X.W., Nishiyama, N.C., Campbell-Beachler, M., Gifford, P., Haynes, K.E., Gridley, D.S., and Pecaut, M.J. (2017). Role of NADPH oxidase as a mediator of oxidative damage in low-dose irradiated and hindlimb-unloaded mice. *Radiat. Res.* *188*, 392–399.
- Mao, X.W., Nishiyama, N.C., Pecaut, M.J., Campbell-Beachler, M., Gifford, P., Haynes, K.E., Becronis, C., and Gridley, D.S. (2016). Simulated microgravity and low-dose/low-dose-rate radiation induces oxidative damage in the mouse brain. *Radiat. Res.* *185*, 647–657.
- Mao, X.W., Sandberg, L.B., Gridley, D.S., Herrmann, E.C., Zhang, G., Raghavan, R., Zubarev, R.A., Zhang, B., Stodieck, L.S., Ferguson, V.L., et al. (2018b). Proteomic analysis of mouse brain subjected to spaceflight. *Int. J. Mol. Sci.* *20*, E7.
- Marcu, O., Lera, M.P., Sanchez, M.E., Levic, E., Higgins, L.A., Shmygelska, A., Fahlen, T.F., Nichol, H., and Bhattacharya, S. (2011). Innate immune responses of *drosophila melanogaster* are altered by spaceflight. *PLoS One* *6*, e15361.
- Martin, J.R., Ernst, R., and Heisenberg, M. (1998). Mushroom bodies suppress locomotor activity in *Drosophila melanogaster*. *Learn. Mem.* *5*, 179–191.
- Mattson, M.P., and Liu, D. (2002). Energetics and oxidative stress in synaptic plasticity and neurodegenerative disorders. *NeuroMolecular Med.* *2*, 215–231.
- McDonald, J., Stainforth, R., Miller, J., Cahill, T., da Silveira, W., Rath, K., Hardiman, G., Taylor, D., Costes, S., Chauhan, V., et al. (2020). NASA GeneLab Platform Utilized for Biological Response to Space Radiation in Animal Models. *Cancers* *12*.
- Mhatre, S.D., Michelson, S.J., Gomes, J., Tabb, L.P., Saunders, A.J., and Maranda, D.R. (2014). Development and characterization of an aged onset model of Alzheimer's disease in *Drosophila melanogaster*. *Exp. Neurol.* *261*, 772–781.
- Miller, M.S., Fortney, M.D., and Keller, T.S. (2002). An infrared system for monitoring *Drosophila* motility during microgravity. *J. Gravit. Physiol.* *9*, 83–91.
- Nelson, G.A. (2016). Space Radiation and Human Exposures, A Primer. *Radiat. Res.* *185*, 349–358. <https://doi.org/10.1667/RR14311.1>.
- Ogneva, I.V., Belyakin, S.N., Sarantseva, S.V., Maximova, M.V., Larina, I.M., Vico, L., and van Loon, J.J. (2016). The development of *Drosophila*

melanogaster under different duration space flight and subsequent adaptation to earth gravity. *PLoS One* **11**, e0166885.

Oliveros, J.C. (2007-2015). Venny. An Interactive Tool for Comparing Lists with Venn's Diagrams.. <https://bioinfogp.cnb.csic.es/tools/venny/index.html>.

Overbey, E.G., Saravia-Butler, A.M., Zhang, Z., Rathi, K.S., Fogle, H., da Silveira, W.A., Barker, R.J., Bass, J.J., Beheshti, A., Berrios, D.C., et al. (2021). NASA GeneLab RNA-seq consensus pipeline: standardized processing of short-read RNA-seq data. *iScience* **24**, 102361.

Parihar, V.K., Allen, B.D., Caressi, C., Kwok, S., Chu, E., Tran, K.K., Chmielewski, N.N., Giedzinski, E., Acharya, M.M., Britten, R.A., et al. (2016). Cosmic radiation exposure and persistent cognitive dysfunction. *Sci. Rep.* **6**, 34774.

Parihar, V.K., Allen, B.D., Tran, K.K., Chmielewski, N.N., Craver, B.M., Martirosian, V., Morganti, J.M., Rosi, S., Vlkolinsky, R., Acharya, M.M., et al. (2015). Targeted overexpression of mitochondrial catalase prevents radiation-induced cognitive dysfunction. *Antioxid. Redox Signal.* **22**, 78–91.

Parihar, V.K., Maroso, M., Syage, A., Allen, B.D., Angulo, M.C., Soltész, I., and Limoli, C.L. (2018). Persistent nature of alterations in cognition and neuronal circuit excitability after exposure to simulated cosmic radiation in mice. *Exp. Neurol.* **305**, 44–55.

R Core Team (2020). R: A language and environment for statistical computing. R Foundation for Statistical Computing, Vienna, Austria. <https://www.R-project.org/>.

Raber, J., Allen, A.R., Sharma, S., Allen, B., Rosi, S., Olsen, R.H.J., Davis, M.J., Eiwaz, M., Fike, J.R., and Nelson, G.A. (2016). Effects of proton and combined proton and <sup>56</sup>Fe radiation on the Hippocampus. *Radiat. Res.* **185**, 20–30.

Raber, J., Torres, E.R.S., Akinyeke, T., Lee, J., Weber Boutros, S.J., Turker, M.S., and Kronenberg, A. (2018). Detrimental effects of helium ion irradiation on cognitive performance and cortical levels of MAP-2 in B6D2F1 mice. *Int. J. Mol. Sci.* **19**, E1247.

Raber, J., Yamazaki, J., Torres, E.R.S., Kirchoff, N., Stagaman, K., Sharpton, T., Turker, M.S., and Kronenberg, A. (2019). Combined effects of three high-energy charged particle beams important for space flight on brain, behavioral and cognitive endpoints in B6D2F1 female and Male mice. *Front. Physiol.* **10**, 179.

Rabin, B.M., Shukitt-Hale, B., Carrihill-Knoll, K.L., and Gomes, S.M. (2014). Comparison of the effects of partial-or whole-body exposures to 16O particles on cognitive performance in rats. *Radiat. Res.* **181**, 251–257.

Rai, B., Kaur, J., Catalina, M., Anand, S.C., Jacobs, R., and Teughels, W. (2011). Effect of simulated microgravity on salivary and serum oxidants, antioxidants, and periodontal status. *J. Periodontol.* **82**, 1478–1482.

Ranjan, A., Behari, J., and Mallick, B.N. (2014). Cytomorphometric changes in hippocampal CA1 neurons exposed to simulated microgravity using rats as model. *Front. Neurol.* **5**, 77.

Ren, X., Zou, L., Zhang, X., Branco, V., Wang, J., Carvalho, C., Holmgren, A., and Lu, J. (2017). Redox signaling mediated by thioredoxin and glutathione systems in the central nervous system. *Antioxid. Redox Signal.* **27**, 989–1010.

Ritchie, M.E., Phipson, B., Wu, D., Hu, Y., Law, C.W., Shi, W., and Smyth, G.K. (2015). Limma powers differential expression analyses for RNA-sequencing and microarray studies. *Nucleic Acids Res.* **43**, e47.

Ronca, A.E., Moyer, E.L., Talyansky, Y., Lowe, M., Padmanabhan, S., Choi, S., Gong, C., Cadena, S.M., Stodieck, L., and Globus, R.K. (2019). Behavior of mice aboard the international space station. *Sci. Rep.* **9**, 10154.

Ross, M.D., and Varelas, J. (2005). Synaptic ribbon plasticity, ribbon size and potential regulatory mechanisms in utricular and saccular maculae. *J. Vestib. Res.* **15**, 17–30.

Roy, C.S., and Sherrington, C.S. (1890). On the regulation of the blood-supply of the brain. *J. Physiol.* **11**, 85–158.17.

Rutter, L., Barker, R., Bezdán, D., Cope, H., Costes, S.V., Degoricija, L., Fisch, K.M., Gabitto, M.I., Gebre, S., Giacomello, S., et al. (2020). A new era for space life science: international standards for space omics processing. *Patterns* **1**, 100148.

Ryczko, D., and Dubuc, R. (2017). Dopamine and the brainstem locomotor networks: from lamprey to human. *Front. Neurosci.* **11**, 295.

Saim, S. (2017). Oxidative stress and the central nervous system. *J. Pharmacol. Exp. Therapeut.* **360**, 201–205.

Shiba, D., Mizuno, H., Yumoto, A., Shimomura, M., Kobayashi, H., Morita, H., Shimbo, M., Hamada, M., Kudo, T., Shinohara, M., et al. (2017). Development of new experimental platform 'MARS'-Multiple Artificial-gravity Research System-to elucidate the impacts of micro/partial gravity on mice. *Sci. Rep.* **7**, 10837.

Slawson, J.B., Kim, E.Z., and Griffith, L.C. (2009). High-resolution video tracking of locomotion in adult *Drosophila melanogaster*. *J. Vis. Exp.*, 1096.

Sokolova, I.V., Schneider, C.J., Bezaire, M., Soltész, I., Vlkolinsky, R., and Nelson, G.A. (2015). Proton radiation alters intrinsic and synaptic properties of CA1 pyramidal neurons of the mouse hippocampus. *Radiat. Res.* **183**, 208–218.

Stein, T.P. (2002). Space flight and oxidative stress. *Nutrition* **18**, 867–871.

Straume, T., Slaba, T.C., Bhattacharya, S., and Braby, L.A. (2017). Cosmic-ray interaction data for designing biological experiments in space. *Life Sci. Space Res.* **13**, 51–59.

Tanner, L.B., Goglia, A.G., Wei, M.H., Sehgal, T., Parsons, L.R., Park, J.O., White, E., Toettcher, J.E., and Rabinowitz, J.D. (2018). Four key steps control glycolytic flux in mammalian cells. *Cell Syst.* **7**, 49–62.e8.

Wallace, D.C. (2005). A mitochondrial paradigm of metabolic and degenerative diseases, aging, and cancer: a dawn for evolutionary medicine. *Annu. Rev. Genet.* **39**, 359–407.

Walls, S., Diop, S., Birse, R., Elmen, L., Gan, Z., Kalvakuri, S., Pineda, S., Reddy, C., Taylor, E., Trinh, B., et al. (2020). Prolonged exposure to microgravity reduces cardiac contractility and initiates remodeling in *Drosophila*. *Cell Rep.* **33**, 108445.

Wang, Y., Iqbal, J., Liu, Y., Su, R., Lu, S., Peng, G., Zhang, Y., Qing, H., and Deng, Y. (2015). Effects of simulated microgravity on the expression of presynaptic proteins distorting the GABA/glutamate equilibrium - a proteomics approach. *Proteomics* **15**, 3883–3891.

Watts, M.E., Pocock, R., and Claudianos, C. (2018). Brain energy and oxygen metabolism: emerging role in normal function and disease. *Front. Mol. Neurosci.* **11**, 216.

White, K.E., Humphrey, D.M., and Hirth, F. (2010). The dopaminergic system in the aging brain of *Drosophila*. *Front. Neurosci.* **4**, 205.

Whoolery, C.W., Walker, A.K., Richardson, D.R., Lucero, M.J., Reynolds, R.P., Beddo, D.H., Clark, K.L., Shih, H.-Y., LeBlanc, J.A., Cole, M.G., et al. (2017). Whole-body exposure to <sup>28</sup>Si-radiation dose-dependently disrupts dentate gyrus neurogenesis and proliferation in the short term and new neuron survival and contextual fear conditioning in the long term. *Radiat. Res.* **188**, 532–551.

Wickham, H. (2016). ggplot2: Elegant Graphics for Data Analysis (Springer-Verlag).

Wilson, M.H., Hargens, A.R., and Imray, C.H. (2018). Effects of spaceflight on astronaut brain structure. *N. Engl. J. Med.* **378**, 581.

Young, L.R. (1999). Artificial gravity considerations for a Mars exploration mission. In *Annals of the New York Academy of Sciences* (New York Academy of Sciences), pp. 367–378.

Yu, G., Wang, L.G., Han, Y., and He, Q.Y. (2012). ClusterProfiler: an R package for comparing biological themes among gene clusters. *Omi. A J. Integr. Biol.* **16**, 284–287.

## STAR★METHODS

### KEY RESOURCES TABLE

REAGENT or RESOURCE	SOURCE	IDENTIFIER
<b>Antibodies</b>		
Anti-Elav	Developmental Studies Hybridoma Bank	Catalog # 7E8A10; RRID:AB_528218
Anti-Cc3	Cell signaling Technology	Catalog # 9661; RRID:AB_2341188
Anti-8-oxo-dG	R&D systems	Catalog # 4354-MC-050; RRID:AB_1857195
Anti-Repo	Developmental Studies Hybridoma Bank	Catalog # 8D12; RRID:AB_528448
Anti-TH	EMD Millipore	Catalog # AB152; RRID:AB_90755
Alexa fluor 568 goat anti-mouse	Invitrogen	Catalog # A-11031; RRID:AB_144696
Alexa fluor 488 goat anti-rabbit	Invitrogen	Catalog # A-11034; RRID:AB_2576217
Alexa fluor 633 goat anti-rat	Invitrogen	Catalog # A21094; RRID:AB_2535749
<b>Experimental models: Organisms/strains</b>		
w <sup>1118</sup>	Bloomington Stock Center	Stock # 3605
<b>Chemicals, peptides, and recombinant proteins</b>		
Phosphate Buffer Saline	Fisher Scientific	Catalog # BP243820
Triton X-100	Thermo-Fisher Scientific	Catalog # A160460F
Normal Goat Serum	Sigma	Catalog # 566380
Vector Shield	Vector Labs	Catalog # H-1000-10
Endoproteinase Lys-C	Wako	Catalog # 125-05061
Trypsin	Promega	Catalog # V5111
C <sub>18</sub> Sep-Pak cartridges	Waters	Catalog # WAT020515
Zorbax 300Extend-C18 column	Agilent	Catalog # 763750-902
Acetonitrile	Fisher	Catalog # A9555
Formic Acid	EMD	Catalog # 1.00264
10mM ammonium bicarbonate	Sigma	Catalog # A6141
<b>Critical commercial assays</b>		
Total RNA was extracted using RNA/Protein Purification plus	Norgen	Catalog# 48200
Bicinchoninic acid assay	Thermo-Fisher Scientific	Catalog # 23275
Thermo-Fisher's TMT 10-plex isobaric label kit	Thermo-Fisher Scientific	Catalog # 90061
<b>Deposited data</b>		
Transcriptomics and Proteomics	NASA/GeneLab	GLDS-514 <a href="https://genelab-data.ndc.nasa.gov/genelab/accession/GLDS-514/">https://genelab-data.ndc.nasa.gov/genelab/accession/GLDS-514/</a>
Inflight behavior analysis	Zenodo	<a href="https://doi.org/10.5281/zenodo.6686815">https://doi.org/10.5281/zenodo.6686815</a>
<b>Software and algorithms</b>		
Matlab	Matlab 2018 (MathWorks, Inc., Natick, MA)	MATLAB; RRID:SCR_001622
Image J v1.52g	U. S. National Institutes of Health, Bethesda, Maryland, USA	ImageJ; RRID:SCR_003070
ggplot2 v3.3.1	<a href="#">Wickham, 2016</a>	<a href="https://ggplot2.tidyverse.org/">https://ggplot2.tidyverse.org/</a> ; RRID:SCR_014601
Trim Galore! v0.6.2	N/A	<a href="https://www.bioinformatics.babraham.ac.uk/projects/trim_galore/">https://www.bioinformatics.babraham.ac.uk/projects/trim_galore/</a> ; RRID:SCR_011847
STAR v2.7.1a	<a href="#">Dobin et al., 2013</a>	<a href="https://github.com/alexdobin/STAR/">https://github.com/alexdobin/STAR/</a> ; RRID: SCR_015899

(Continued on next page)

**Continued**

REAGENT or RESOURCE	SOURCE	IDENTIFIER
RSEM v1.3.1	Dobin et al., 2013	<a href="https://deweylab.github.io/RSEM/">https://deweylab.github.io/RSEM/</a> ; RRID: SCR_013027
DESeq2 v1.22.2	Love et al., 2104	<a href="https://github.com/mikelove/DESeq2">https://github.com/mikelove/DESeq2</a> ; RRID: SCR_01568
pheatmap v1.0.12	Kolde, 2015	<a href="https://github.com/raivokolde/pheatmap">https://github.com/raivokolde/pheatmap</a> ; RRID:SCR_016418
R package v3.6.1 and v4.0.1	R Core Team, 2020	<a href="https://www.r-project.org/">https://www.r-project.org/</a> ; RRID:SCR_001905
Proteome Discoverer v2.1	Thermo Fisher Scientific	Proteome Discoverer; RRID:SCR_014477
Limma v3.44.3	Ritchie et al., 2015	<a href="https://www.bioconductor.org/packages/release/bioc/html/limma.html">https://www.bioconductor.org/packages/release/bioc/html/limma.html</a> ; RRID: SCR_010943
ClusterProfiler v 3.18.0	Yu et al., 2012	clusterProfiler; RRID:SCR_016884
Venny 2.1	Oliveros J. C. (2007-2015)	<a href="http://bioinfogp.cnb.csic.es/tools/venny/">http://bioinfogp.cnb.csic.es/tools/venny/</a> ; RRID:SCR_016561
<b>Other</b>		
Illumina Novaseq 6000	Illumina, San Diego, CA	<a href="https://www.illumina.com">https://www.illumina.com</a>
Ultimate 3000 HPLC	Thermo Scientific	<a href="https://www.thermofisher.com">https://www.thermofisher.com</a>
Dionex Ultimate 3000	Thermo Scientific	<a href="https://www.thermofisher.com">https://www.thermofisher.com</a>
UltiMate 3000 RSLCnano system	Thermo Scientific	<a href="https://www.thermofisher.com">https://www.thermofisher.com</a>
Orbitrap Fusion mass spectrometer	Thermo Scientific	<a href="https://www.thermofisher.com">https://www.thermofisher.com</a>

**RESOURCE AVAILABILITY**

**Lead contact**

Further information and requests for resources should be directed to and will be fulfilled by the lead contact, Sharmila Bhattacharya ([sharmila.bhattacharya@nasa.gov](mailto:sharmila.bhattacharya@nasa.gov)).

**Materials availability**

This study did not generate new unique reagents.

**Data and code availability**

- All data reported in this paper will be shared by the **lead contact** upon request. Transcriptomic and proteomic data (Raw read counts and FASTQ files) are made available at the community-endorsed public repository at NASA Gene Lab Database: <https://genelab-data.ndc.nasa.gov/genelab/accession/GLDS-514/>
- The code generated during this study is openly available on Zenodo: <https://doi.org/10.5281/zenodo.6686815>.
- Any additional information required to reanalyze the data reported in this paper is available from the **lead contact** upon request.

**EXPERIMENTAL MODEL AND SUBJECT DETAILS**

**Spaceflight mission and hardware description**

The MVP-Fly01 mission (Figures 1A and 1B) was launched on SpaceX-14 to the ISS at 20:30 UTC (Coordinated Universal Time) on April 2<sup>nd</sup>, 2018. Flies were kept in the MVP hardware throughout the 34-day mission on the ISS (Figure S1A). The Dragon capsule was unberthed at 13:22 UTC on May 5th, 2018, and splashdown in the Pacific Ocean was the same day at 20:00 UTC. The mission used the MVP hardware (Redwire/Techshot, Inc., Greenville, Indiana) that supports easy food changes, allowing for a large population of flies to be maintained over multiple generations. It is also equipped with UI-1491LE video cameras used to capture time course footage of *D. melanogaster* (Figure S1B). The hardware consists of uniform white LED illumination which was programmed for a 12-h:12-h (light: dark) cycle for each habitat. Fresh cabin air was continuously circulated through the habitat to maintain steady CO<sub>2</sub> and O<sub>2</sub> levels. The housing system consists of two independent centrifuge units maintained within the same habitat enclosure, each containing six MVP modules (Figures S1A and S1B). For this experiment, one centrifuge was rotated at 68 rpm to artificially simulate Earth's gravity (SF1g) in space. The other centrifuge was rotated at 2.2 rpm, making the g-level at the outer edge of the carousel at approximately 0.00095g (SF<sub>μ</sub>g). This minimal rotation of SF<sub>μ</sub>g ensured temperature uniformity between all experimental modules, while maintaining the microgravity levels of the ISS. Each MVP module has two adult fly chambers and three food cylinders

(Figure S1B). Each food cylinder holds approximately 9.2 mL of standard fly food (Gilbert et al., 2020) containing food-grade blue food dye. The presence of the dye allowed for the differentiation between early and late third-instar larvae during postflight specimen sorting. Its inclusion is not relevant to the current analysis of adult flies performed here. The hardware design allowed for the passage of two generations of flies sequentially from adult fly chamber 2 to adult fly chamber 1 (Figure S1B). The MVP hardware has video imaging capabilities, and 28-second video footage of the adult fly chambers was taken regularly throughout the 12-h light period. Although the MVP hardware has night video recording capability, it was not utilized in this mission due to technical difficulties with the infrared lighting.

Each 28-s video consisted of 368 frames with an image resolution of 1986 × 1064 pixels. This video was periodically checked during the mission to ensure the health of flies and gauge the overall well-being. Upon return, this video was analyzed for inflight behavior to compute adult fly activity in SF1g and SF $\mu$ g conditions during the mission. Following the completion of the mission, the samples were returned to Port of Long Beach, California, and transported via a climate-controlled vehicle to NASA Ames Research Center (ARC), California, within 7 h of landing. Temperature and humidity loggers were also programmed to monitor the samples throughout the journey. All dissections, fixation of brain tissue, and postflight behavioral analysis (described below) were performed within 24 h of arrival at NASA ARC (Return+0 days = R+0). A small subset of flies separated by sex was placed in an incubator at 24°C for acclimation to earth condition for 25 days (Return+25 days = R+25), and the brains from these flies were processed for immunohistochemical analysis similar to R+0 flies (Figure 1B).

During the mission, a small set consisting of only two MVP modules (synchronous control) was reared in a ground-based incubator with real-time changes in temperature, humidity, and CO<sub>2</sub> matching the telemetry recorded on the ISS. The synchronous control was checked periodically to ensure the overall health of the flies during the mission but was not used for any of the postflight analysis. Upon completing the mission, a postflight ground control with the same hardware used for the mission was conducted in a ground-based incubator with six MVP modules resulting in 883 flies. For the postflight control (Earth), flies were placed in each module to match the flight condition and were reared under identical conditions to match the temperature, relative humidity, O<sub>2</sub>, and CO<sub>2</sub> levels recorded for the entire experiment on the ISS. The CO<sub>2</sub> levels within habitats in space are often significantly higher than those on the ground due to the technical difficulty of scrubbing the CO<sub>2</sub> from an entirely enclosed environment (ISS). The average CO<sub>2</sub> level in the MVP hardware during this experiment ranged between 3500 and 5443 ppm during the mission and was replicated temporally and identically in the ground control. By comparison, the CO<sub>2</sub> level under regular laboratory conditions averages <1000 ppm (Hussin et al., 2017). Also, another variable in any spaceflight study is sound pressure level. Based on ISS's telemetry data and payload permissible limits, SF1g and SF $\mu$ g flies in the MVP module on ISS experienced average sound pressure levels of 65dB. Similar sound pressure levels (62–65dB) were noted in the vicinity of the Earth controls placed in the laboratory incubator (Percival Scientific). The Earth control flies were fixed in RNAlater and subjected to postflight analyses following the same timeline as the flies from ISS. The Earth control used for comparison and statistical analysis in this manuscript is this postflight ground control.

### Fly husbandry, loading the module, and development

The *w<sup>1118</sup>* wildtype line (Bloomington Stock Center) was used in this study. Thirty hours prior to launch, one-day-old virgin male (10) and female (25) fruit flies were loaded into the adult food cylinder 3 in each of the six MVP modules (F0 generation). The food cylinder was then immediately opened to adult fly chamber 2 (Figures S1B and S1C). The modules were then placed inside of a standard cargo transfer bag for launch. Prepared food cylinders were stored at 4°C for the duration of launch and ISS operations. Approximately 3.7 days (90 h) after launch, the payload was delivered to the ISS and the crew installed a food cylinder 2 inside the MVP module and opened the food cylinder 2 to adult fly chamber 2 (Mission day = 5), giving flies access to the new food. Food cylinder 3 was closed at this time. This procedure was repeated for all MVP modules, and the modules were loaded into the previously installed MVP habitat hardware (Figure S1A) by the ISS crew. At this time, the six SF1g modules started spinning at 68 rpm to maintain 1g in spaceflight while the six SF $\mu$ g modules were maintained at microgravity levels.

After 5.5 days of egg laying (Mission Day = 10), food cylinder 2 was opened to adult fly chamber 1 to allow the eggs laid in space to develop and emerge into adult flies in chamber 1. At the same time food cylinder 2 was closed to adult fly chamber 2, such that the launch populations of flies were prevented from entering food cylinder 2, thus keeping the generations separated (Figure S1C). Food cylinder 3 was reopened to adult fly chamber 2 to continue providing food to this population for the remainder of the experiment. The larvae and flies that emerged from the food cylinder 2 into the adult fly chamber 1 had undergone their entire developmental life cycle during spaceflight (F1 generation). At this time, food cylinder 1 was inserted and opened to chamber 1 to allow egg laying in cylinder 1, which will produce the second generation of spaceflight-developed flies (F2 generation). Food cylinder 2 remained open to chamber 1 during egg lay to allow adults to continue emerging. This also allowed us to know the age range of the adult flies returned for postflight experiments (~11–17-day adults).

After 8 days of egg laying, food cylinder 1 from each module containing F2 generation fruit fly eggs and larvae, and some F1 generation adults, was fixed in RNAlater (Invitrogen). This allowed us to have samples that were fixed in RNAlater in space for “omics” analyses on the ground to track the progression of acclimation to spaceflight as animals develop in space under different gravity conditions. Following the fixation, a fresh food cylinder 1 was inserted and opened to chamber 1, and food cylinder 2 was closed. The MVP locker was powered down after the experiment, and fixed F1 generation flies and F2 generation eggs and larvae were placed in the MELFI-2 freezer at –80°C until the samples returned. Thus, this experimental design allowed us to freeze adult flies (F1 generation), larvae (F2 generation), and eggs (F2 generation) at Day 29. Postflight, we retrieved live adult flies (F1 generation), and eggs and

larvae of F2 generation in the new food cylinder 1. All the science operations, including food cylinder changes and fixation and opening/closing of chambers, were performed by the ISS crew. Unforeseen weather conditions delayed the mission by 4 days, during which the crew repowered the MVP hardware on mission day 31 and powered it off on mission day 34 for return to Earth.

## METHOD DETAILS

### Inflight behavioral analysis

To quantify fly activity on the ISS, a simple but robust algorithm was developed using image-processing techniques in Matlab 2018 (MathWorks, Inc., Natick, MA) and DIPimage (Luengo Hendricks et al., 1999) running on a MacBook Pro with an i7 core processor. Only the videos from adult fly chamber 1 SF1g and SF $\mu$ g were analyzed in this study (Mission days 13–28 –Figure S1C) since these chambers contained the flies bred entirely in space (F1 generation). The age of the flies assessed from video imaging of the inflight behavior ranged from 1 to 16-days (Postflight assays were conducted with flies with a smaller age range as described in the relevant sections). Similar video recording arrangements were made for Earth condition, but the videos could not be recorded due to technical issues. Full resolution 8-bit images (1986x1064) were used for analysis. The individual frames from the video images have a predominant intensity in the blue channel (Figure 1C.i). Therefore, each video image was separated into its three RGB components, and the blue channel (shown in grayscale) was inverted and used for further analysis (Figure 1C.ii) as it provided best visualization of the flies. Once inverted, resulting images had individual flies that appeared as white pixels on a gray background. For each movie, maximum intensity projections (MIP) were computed by overlaying individual video frames and keeping the brightest pixels across all time points, resulting in a stroboscopic motion-like effect (Figure 1C.iii and 1C.iv). The pixel location of the MIP was mapped on a composite image to visualize the locomotion of individual flies during each video. These tracks had a higher intensity and appeared brighter than the background. Flies that did not move did not create a track, as seen between Figure 1C.ii and 1C.iii indicated in green. However, flies that were active during the video recording created a white track, shown in Figure 1C.ii and 1C.iii in blue and red. This process resulted in a single image that displayed the tracks of the fly population throughout a series of 28-s video recordings (Figure 1C.iv).

Using the MIP images of adult fly chamber 1, we could determine when flies were active. The videos from mission day 13 to 28 (Figure S1C) that tracked the F1 generation of flies as shown in Figures 1D and 1E. In other words, this time frame included initial fly emergence when the majority of the space-bred generation of flies entered adult fly chamber 1 from food cylinder 2 but ended prior to fly numbers and debris levels increasing to a point where the camera view was obstructed (Figure S2). The number of flies in a chamber increased over time due to reproduction based on the life cycle of *D. melanogaster* (Fernández-Moreno et al., 2007) (Figure S2). Six videos per day, each 28 s in duration that spanned the 12-h light period, were processed to produce MIP images for each fly module. One of the six modules containing the population bred in  $\mu$ g malfunctioned during flight, so our analysis includes six modules in SF1g and five modules in SF $\mu$ g. Videos from adult fly chamber 2 were not used for analysis because 1) the build-up of debris due to more extended periods of growth compared to adult fly chamber 1 obscured the camera view, and 2) the chamber contained mixed generations of flies. The pixel intensities were summed for each MIP image, resulting in a single numerical value for every video. The more a fly moves, the longer are the white streaks that can be observed along its path on the MIP and the higher is the total measured intensity. The process was repeated for each video producing a series of numerical values to quantify the overall activity of the fly population during the mission. Video S1 and S2 is a representative video showing the fly chambers of SF1g and SF $\mu$ g, where suspended flies are seen in microgravity condition. The color map in Figure 1D was generated by setting the minimum value in the color map to the baseline intensity obtained from the first frame of the video. The intensities across all modules and treatments were scaled such that the video with the MIP image having the highest summated intensity (and therefore highest activity) was set to the maximum color on the color scale (Figure 1D). Note: No videos were analyzed for activity past day 28 due to the increased fly numbers and debris interfering with the image quality.

### Climbing assay

Climbing assay was performed on F1 generation of flies returned to Earth using a modified version of Le Bourg and Lints (Feany and Bender, 2000). For each condition, flies were sorted and collected by sex, in groups of ten per food vial (F100, M = 100) as soon as the live flight samples were returned on earth (i.e., Figure 1B, splash at L+34, 2 days for samples turnover (Long Beach, CA) and arrived at NASA ARC (R+0) and the assay was conducted. During the climbing assay, flies were transferred to a clean, empty vial and allowed to adjust for 1 min. The flies were tapped down to the bottom, and the number of flies climbing past the 5 cm mark measured from the bottom of the vial in 18 s was recorded as a percentage of flies able to climb per vial (climbing ability). This assay was repeated three times for each vial, with a 30 s rest between trials. An average of three trials was reported per vial. Measurements from all three trials were averaged. The significance was determined between the conditions by a one-way ANOVA analysis with the condition as the independent variable.

### Immunohistochemistry and confocal imaging of brains

F1 generation flies returned live were dissected (R+0 and R+25) and brains were immediately fixed for 20 minutes in PBS (Phosphate buffered saline) containing 4% paraformaldehyde, 6.7% sucrose, and 0.01% tween-20, and stored at 4°C in PBS with 0.05% sodium azide. The R+0 and R+25 brains were stained for immunohistochemical analysis (described below) where staining for different

antibody markers was conducted at the same time to facilitate comparison and reduce variability. The brains were stained following a standard protocol (Iyer et al., 2018; Mhatre et al., 2014). Briefly, the fixed brains were washed with PBS and PBT (0.2% Triton X-100 in PBS) for 10 min each, incubated with blocking buffer (5% normal goat serum (Catalog # 566380, Sigma) in PBT) for one hour, and then incubated overnight at 4°C with primary antibodies. One set of brains were stained with anti-elav (1:100, Catalog # 7E8A10, Developmental Studies Hybridoma Bank (DSHB), host species - rat) to label all the neurons, anti-cc3 (1:100, Catalog # 9661, Cell signaling Technology, host species - rabbit) as apoptotic marker, and anti-8-oxo-dG (1:100, Catalog # 4354-MC-050, R&D systems, host species - mouse) as the DNA oxidative damage marker. Another set of brains were stained with anti-Repo (1:50, Catalog # 8D12, DSHB), University of Iowa, host species - mouse) to label the glia, and anti-TH (1:300, Catalog # AB152, EMD Millipore, host species - rabbit) to label the dopaminergic neurons. These preparations were then washed three times with PBT for 10 min each, and incubated with fluorophore-conjugated secondary antibodies, Alexa fluor 568 goat anti-mouse (1:200; Catalog # A-11031, Invitrogen), Alexa fluor 488 goat anti-rabbit (1:200; Catalog # A-11034, Invitrogen), or Alexa fluor 633 goat anti-rat (1:200; Catalog # A21094, Invitrogen). Final washes were performed once with PBT and twice with PBS, each for 10 min, and mounted in Vectashield (Vector Labs, H-1000) for imaging.

Stained brains were imaged using Zeiss LSM 880 laser scanning confocal microscope in the histology and microscopy core facility at the Gladstone Institute, University of California San Francisco (UCSF). The ELAV neuronal cortex, neuropil, and the total brain area were traced and quantified using Image J software (v1.52g, U. S. National Institutes of Health, Bethesda, Maryland, USA). This method is a gross measurement adapted from previously published papers (Chakraborty et al., 2011; Mhatre et al., 2014). The data reported here are the neuronal cortex and neuropil area normalized to the total brain area. Similarly, the number of puncta for TH (total number of TH-positive cells), repo, 8-oxo-dG, and CC3 were analyzed and quantified for each stain/marker using the cell counter in ImageJ software and are reported as absolute values.

### RNA isolation, sequencing, and analysis of fly heads

The food cylinders that were frozen on ISS were slow-thawed at 4°C before opening. Once thawed, cylinders were opened, and flies (F1 generation frozen at L+29 days) were removed and sorted by sex. The head was removed using spring scissors and placed in RNAlater to preserve the RNA and protein integrity. Total RNA was extracted using RNA/Protein Purification plus (Norgen) from adult heads with four biological replicates in each condition (12–15 heads per replicate). This kit isolated total RNA and protein from the same samples. Isolated RNA was used to perform paired-end RNA sequencing on Illumina Novaseq 6000 platform, with an average of 20M reads of PE150 per sample (Novogene, Sacramento, CA). Data validation and quality control with FASTQC were conducted by Novogene, Inc. The standardized Genelab pipeline was used for the analysis (Overbey et al., 2021). Briefly, raw RNA sequences were trimmed using Trim Galore! v0.6.2, aligned to the *Drosophila* reference genome (Dmel release 6.08) and transcriptome with STAR Version 2.7.1a (Dobin et al., 2013), and read counts for each transcript were generated using RSEM v1.3.1. Differentially expressed gene lists were generated using a custom Genelab R script, GeneLab\_DGE\_noERCC.R, utilizing the DESeq2 v1.22.2 R package (Lai Polo et al., 2020). False discovery rate (adjusted p value) corrections were performed using Benjamini-Hochberg multiple testing adjustment, and the differentially expressed genes with an adjusted p value of less than 0.05 were considered statistically significant.

### Proteomics and analysis of fly heads

Proteins isolated from adult heads (F1 generation frozen at L+29 days) using the Norgen Biotek kit were used to determine the global proteomic changes. Three replicates in each condition (12–15 heads per replicate) were used for protein isolation and enzymatic digestion. Isolated protein samples were digested and desalted according to Lundby et al. (Lundby et al., 2012). Protein concentrations were then determined using a bicinchoninic acid assay (BCA) (Thermo-Fisher Scientific, San Jose, CA). Proteins were then reduced, alkylated and subjected to acetone precipitation prior to digestion with endoproteinase Lys-C, 1:50 enzyme to protein (Wako, Richmond, VA). This was followed by digestion with trypsin, 1:50 enzyme to protein (Promega, Madison, WI), and desalting and concentrating using C<sub>18</sub> Sep-Pak cartridges (Waters).

### TMT isobaric labeling

Peptides were mass tagged using Thermo-Fisher's TMT 10-plex isobaric label kit (Catalog # 90,061) following the included protocol and pooled for analysis. Six experimental conditions were labeled in triplicate across three TMT-runs, including two internal control channels.

### Basic reversed-phase fractionation

Pooled TMT-labeled peptides were fractionated by basic pH reversed-phase (BPRP) fractionation on an Ultimate 3000 HPLC (Thermo Scientific) using an integrated fraction collector. Elution was performed using a 10-min gradient of 0–20% solvent B followed by a 50-min gradient of solvent B from 20 to 45% (Solvent A 5.0% Acetonitrile, 10mM ammonium bicarbonate pH 8.0, Solvent B 90.0% Acetonitrile, 10mM ammonium bicarbonate pH 8.0) on a Zorbax 300Extend-C18 column (Agilent) at a flow rate of 0.4 mL/min. A total of 24 fractions were collected at 37-s intervals in a looping fashion for 60 min then combined to produce 12 super fractions. Peptide elution was monitored at a wavelength of 220nm using a Dionex Ultimate 3000 variable wavelength detector (Thermo Scientific). Each fraction was then centrifuged to near dryness and desalted using C<sub>18</sub> Sep-Pak Cartridges followed again by centrifugation to near dryness and reconstitution with 20 ul of 5% acetonitrile and 0.1% formic acid.

### Liquid chromatography and mass spectrometry

BPRP fractions were then separated using an UltiMate 3000 RSLCnano system (Thermo Scientific, San Jose, CA) on a self-packed C18 column (100  $\mu\text{m}$   $\times$  35 cm). Separation was performed using a 180-min gradient of solvent B from 2–27% (Solvent A 0.1% Formic Acid, Solvent B Acetonitrile, 0.1% Formic Acid) at 50°C using a digital PicoView nanospray source (New Objectives, Woburn, MA) that was modified with a custom-built column heater and an ABIRD background suppressor (ESI Source Solutions, Woburn, MA). An in-house column was prepared by packing a 100  $\mu\text{m}$  inner diameter picofrit column (New Objectives, Woburn, MA) with 1.9  $\mu\text{m}$  ReproSil-Pure C18 (Dr. Maisch, Ammerbuch, Germany) and packed to a length of 30 cm at 9000 psi using a nano-LC column packing kit (nanoLCMS, Gold River, CA).

Mass spectral analysis was performed using an Orbitrap Fusion mass spectrometer (Thermo Scientific, San Jose, CA). TMT analysis was performed using an MS3 multi-notch approach. The MS1 precursor selection range is from 400–1400  $m/z$  at a resolution of 120K and automatic gain control (AGC) target of  $2.0 \times 10^5$  with a maximum injection time of 100 ms. Quadrupole isolation at 0.7 Th for MS<sup>2</sup> analysis using CID fragmentation in the linear ion trap with a collision energy of 35%. The AGC was set to  $4.0 \times 10^3$  with a maximum injection time of 150ms. The instrument was operated in a top-speed data-dependent mode with a most intense precursor priority with dynamic exclusion set to an exclusion duration of 60 s with a 10ppm tolerance. MS2 fragment ions were captured in the MS3 precursor population. These MS3 precursors were then isolated within a 2.5 Da window and subjected to high energy collision-induced dissociation (HCD) with a collision energy of 55%. The ions were then detected in the Orbitrap at a resolution of 60,000 with an AGC of  $5.0 \times 10^4$  and a maximum injection time of 150 ms. The data was then analyzed using SEQUEST (Thermo Fisher Scientific, San Jose, CA, version v.27, rev. 11.) and Proteome Discoverer (Thermo Scientific, San Jose, CA, version 2.1).

### Database searching

Tandem mass spectra were extracted, and charge states were deconvoluted by Proteome Discoverer version 2.1. Assignment of MS/MS spectra was performed using SequestHT (Thermo Fisher Scientific, San Jose, CA, USA) by searching the data against a protein database, including all entries from the Uniprot *Drosophila* proteome (UniProt UP00000803, containing 21,041 sequences, download date 10-29-2019) combined with the common contaminants sequences from the Global Proteome Machine. Sequest searches were performed using a parent ion tolerance of 1.25 Da, fragment ion mass tolerance of 1.00005 Da, and requiring each peptides' termini to have trypsin protease specificity while allowing up to two missed cleavages. Carbamidomethylation of cysteine residues (+57.02146 Da) was set as static modification, while TMT tags on peptide N termini/lysine residues (+229.162932 Da), acetylation of the protein N-terminus, and methionine oxidation (+15.99492 Da) was set as variable modification. Reporter Ions Quantifier settings were set to include unique and razor peptides, Quan value correction factors from manufacturer applied, co-isolation threshold 50%, average reporter S/N 10, and no normalization or scaling of the channels.

### Proteomic data analysis

The unscaled, non-normalized protein-level total reporter ion intensities derived from unique peptides were exported from Proteome Discoverer. Data quality assessment and control, normalization and analyses were performed using R v 4.0.1. Proteins underwent three filtering steps: 1) proteins containing missing values in any condition, 2) proteins with fewer than two unique peptide matches, and 3) proteins identified in only one or two out of the three runs were excluded from the quantitative analysis. Each TMT run was internally scaled, then transformed and analyzed together. Merged data were greatly affected by commonly seen batch effects associated to individual runs. Bioconductor package Limma v 3.44.3 was used to identify sex-specific abundance differences per protein in response to changing gravity conditions relative to ground/earth control by performing an empirical Bayes moderated  $t$ -test accounting for the seen batch effect caused by each individual TMT run (Ritchie et al., 2015). Calculated p-values were corrected by Benjamini–Hochberg False Discovery Rate (FDR). Statistically significant difference was defined by an FDR cutoff of 0.05.

### Gene ontology and KEGG analysis

The differentially expressed genes and proteins with FDR adjusted p-values less than 0.05 were used for further analysis. Gene ontology (GO) and KEGG enrichment analyses were performed using Bioconductor package ClusterProfiler v 3.18.0 (Yu et al., 2012) and *Drosophila* database (org.Dm.eg.db version 3.13). Specifically, we used enrichGO and enrichKEGG functions to determine functionally enriched GO categories for are three annotations: biological process (BP), cellular component (CC), and molecular function (MF) and KEGG pathways (Carbon et al., 2021) for all contrasts across both transcriptomics and proteomics datasets. Results were visualized by R packages ggplot2 (Wickham, 2016) and pheatmap (Kolde, 2015). The intersecting genes and proteins within and across the multi-omics platform were plotted using the Upset plot (Khan and Mathelier, 2017). Pathway visualization was performed using the KEGG mapper function provided by Kanehisa Laboratories (<https://www.kegg.jp/>). Venn diagrams were generated using Venny 2.1 (Oliveros J. C. 2007–2015).

## QUANTIFICATION AND STATISTICAL ANALYSIS

Quantification methods for the various assays and parameters are described in the relevant STAR methods section. Statistical analyses and plot generation were performed using GraphPad Prism software (v. 9.1.0). For Figure 1E, two-tailed Student's  $t$ -test was performed to determine statistical significance. Grubbs test was performed on all climbing and immunohistochemistry datasets to remove outliers. In Figures 2 and 6 (A–C, F), S3A, and S7, Grubbs test was followed by testing for normal Gaussian distribution via the D'Agostino–Pearson test except in data with a low sample size (TH and Repo), where the Shapiro–Wilk test for normality was



performed. If data were normally distributed, a two-way ANOVA, followed by Tukey's multiple comparison test, was performed to determine statistical significance. \* $p < 0.05$ , \*\* $p < 0.01$ , \*\*\* $p < 0.001$ .

For [Figures 6D and 6A](#) non-parametric t -test (Mann-Whitney test) was performed to compare all conditions (Earth, SF1g, and SF $\mu$ g) within their respective time points (R+0, R+25). A value of  $p < 0.05$  was considered statistically significant. The error bars in the figures represent SEM (Standard Error Mean). All data are means  $\pm$  SEM ( $p < 0.05$ ,  $n = 5-12$  per group). The number of flies used per experiment is indicated in the figure legend. Inflight behavior analysis was conducted by composing Matlab code using Matlab 2018 (MathWorks, Inc., Natick, MA) and DIPimage ([Luengo Hendricks et al., 1999](#)).